



Modelling, singular perturbation and bifurcation analyses of bitrophic food chains

B.W. Kooi, J.C. Poggiale

► To cite this version:

B.W. Kooi, J.C. Poggiale. Modelling, singular perturbation and bifurcation analyses of bitrophic food chains. *Mathematical Biosciences*, 2018, 301, pp.93-110. 10.1016/j.mbs.2018.04.006 . halshs-01778648

HAL Id: halshs-01778648

<https://shs.hal.science/halshs-01778648>

Submitted on 23 Feb 2019

HAL is a multi-disciplinary open access archive for the deposit and dissemination of scientific research documents, whether they are published or not. The documents may come from teaching and research institutions in France or abroad, or from public or private research centers.

L'archive ouverte pluridisciplinaire **HAL**, est destinée au dépôt et à la diffusion de documents scientifiques de niveau recherche, publiés ou non, émanant des établissements d'enseignement et de recherche français ou étrangers, des laboratoires publics ou privés.

Modelling, singular perturbation and bifurcation analyses of bitrophic food chains

B.W. Kooi* and J.C. Poggiale**,

* Faculty of Science, VU Amsterdam,
De Boelelaan 1085,

1081 HV Amsterdam, The Netherlands.

** Aix-Marseille University, UMR 7294 MIO OCEANOMED,
Campus de Luminy, 163 Avenue de Luminy case 901,
13009 Marseille, France.

March 15, 2018

Abstract

Two predator-prey model formulations are studied: for the classical Rosenzweig-MacArthur (RM) model and the Mass Balance (MB) chemostat model. When the growth and loss rate of the predator is much smaller than that of the prey these models are slow-fast systems leading mathematically to singular perturbation problem. In contradiction to the RM-model, the resource for the prey are modelled explicitly in the MB-model but this comes with additional parameters. These parameter values are chosen such that the two models become easy to compare. In both models a transcritical bifurcation, a threshold above which invasion of predator into prey-only system occurs, and the Hopf bifurcation where the interior equilibrium becomes unstable leading to a stable limit cycle. The fast-slow limit cycles are called relaxation oscillations which for increasing differences in time scales leads to the well known degenerated trajectories being concatenations of slow parts of the trajectory and fast parts of the trajectory. In the fast-slow version of the RM-model a canard explosion of the stable limit cycles occurs in the oscillatory region of the parameter space. To our knowledge this type of dynamics has not been observed for the RM-model and not even for more complex ecosystem models. When a bifurcation parameter crosses the Hopf bifurcation point the amplitude of the emerging stable limit cycles increases. However, depending of the perturbation parameter the shape of this limit cycle changes abruptly from one consisting of two concatenated slow and fast episodes with small amplitude of the limit cycle, to a shape with large amplitude of which the shape is similar to the relaxation oscillation, the well known degenerated phase trajectories consisting of four episodes (concatenation of two slow and two fast).

The canard explosion point is accurately predicted by using an extended asymptotic expansion technique in the perturbation and bifurcation parameter simultaneously where the small amplitude stable limit cycles exist. The predicted dynamics of the MB-model is in a large part of the parameter space similar to that of the RM-model. However, the fast-slow version of MB-model does not predict a canard explosion phenomenon.

Keywords:

Aggregation methods; Asymptotic series expansion; Canard; Geometrical Singular Perturbation theory; Predator-prey models

Mathematics Subject Classification: 34E17 - 37G15 - 92D25 - 92D40

1 Introduction

There is already a long tradition in modelling predator–prey systems under various environmental conditions. In some realistic cases there are differences in the order of magnitudes of the ingestion and growth rates of the two populations leading to so called fast-slow dynamical systems. Various mathematical analyses techniques have been used to analyse these models. Here we focus on the application of perturbation techniques when the processes of the two population occur at different time-scales.

The starting point is the Rosenzweig-MacArthur (RM) model [44] where the prey population grows logistically and the predator-prey interaction is described by the Holling type II functional response. This predator-prey system is mathematically described by two ordinary differential equations, (ODE)s, for the prey and the predator population. This model does not obey mass conservation law, however. Therefore we study also a version where additionally the prey population consumes abiotic nutrients. The resulting model is called the Mass Balance (MB) model where mass conservation is obeyed. This type of model is common practice in modeling food chains in a chemostat reactor which have been studied extensively: we refer to [45, 24]. These systems consist minimally of a nutrient, a prey and a predator. Consequently, the description of the dynamics involves three ODEs. The resulting three dimensional model is reduced to a two dimensional model for prey and predator populations when realistic assumptions are made.

For both types of models it is well known that the long-term dynamics is either a stable equilibrium (boundary: prey only, or interior: predator-prey) or a stable predator-prey limit cycle. For the RM-model, in [19] it was proved that the coexistence equilibrium is globally stable and in [4] that the periodic solution is unique thus a globally stable limit cycle and in [31] a detailed bifurcation analysis is performed.

Nutrient enrichment leads to the risk of extinctions when fluctuating densities during the limit cycle reach low values, called the “paradox of enrichment” [43]. Mathematically the first transition occurs at a transcritical bifurcation and the second at a Hopf bifurcation. This holds for both types of model the RM and MB-model.

When the growth and loss rate of the predator is much smaller than that of the prey, the system becomes a so called slow–fast system. These rates for the predator are multiplied by a perturbation parameter. These systems have been studied intensively in the literature, the RM-model with fast-slow dynamics in [35, 42, 41, 5, 11]. Slow-fast systems can naturally be identified, are often encountered in ecology. This is almost a rule when behavioral and population dynamics are considered at the same time. But also interactions between two populations like plankton and fish, plants and insects, herbs and trees are classical examples of systems with two time scales (see [41]). Another example where there are differences in the order of magnitudes of the ingestion and growth rates is a food chain of sewage-bacterium-worms often found in wastewater treatment plants (see [40]). The worm is the water nymph *Nais elinguis*, a oligochaete species. In a previous paper [25] we took advantage of these different time scales to apply aggregation methods in order to simplify the models for the dynamics of the wastewater treatment plant system.

Using a perturbation technique often the slow variables are frozen with the calculation

of the equilibria of the fast system but better approximations are obtained by asymptotic expansions [18, 16]. When the perturbation parameter becomes small the resulting limit cycle is called the *relaxation oscillation*, see [15], where the periodic orbits are phase plane curves with both fast and slow parts of the trajectory.

When the time-scales differences are very large, that is with small positive perturbation parameter, the presence of the Hopf bifurcation indicates the possible occurrence of so called *canards*. In physics this has been studied extensively for the van der Pol equations [47, 10, 6, 3, 8, 28, 29, 2]. More recently, in [37, 16] geometric singular perturbation techniques [12] have been studied for application in biological practice, including these slow-fast predator-prey systems. In this theory *invariant manifolds* play an important role in the study of structural stability of dynamical systems or, when a degeneracy occurs, in understanding the nature of bifurcations. A trajectory is an example of an invariant manifold. Using this approach we will find that similar to the van der Pol equations case also for the RM-model application of asymptotic expansions [3, 2] for the critical manifolds leads to a divergent expansion. Nevertheless we will show that we are still able to compute for which bifurcation parameter values a canard explosion occurs.

Bifurcation analysis results show that in the MB-model the singularity in the limiting time-scale differences is completely different from that in the RM-model where the prey grows logistically. Only local bifurcations occur and therefore continuation of equilibrium and limit cycles gives a full picture of the long-term dynamics.

2 The RM bitrophic food chain model

A standard two-level food chain model from the field of theoretical biology is the scaled Rosenzweig-MacArthur system (1963). The RM-model reads in dimensionless form derived in the Appendix A:

$$\frac{dx_1}{dt} = x_1 \left(1 - x_1 - \frac{a_1 x_2}{1 + b_1 x_1} \right), \quad (1a)$$

$$\frac{dx_2}{dt} = x_2 \left(\frac{c_1 a_1 x_1}{1 + b_1 x_1} - d_1 \right), \quad (1b)$$

with $x_i(t) \in \mathbb{R}_+$, $t \geq 0$, $i = 1, 2$, respectively the size of the prey and predator population. The first part of (1a) models that the prey population grows logistically in absence of the predator. The hyperbolic relationship $a_1 x_1 / (1 + b_1 x_1)$ is called the Holling type II functional response. This expression occurs in both equations and models the consumption of the prey population by the predator population. Parameter $a_1 > 0$ is the searching rate for the prey and $b_1 > 0$ the product of the handling time of the prey by the predator and the searching rate. The ratio of the first term of (1b) and the last term on the right-hand sides of (1a) is the efficiency $c_1 > 0$. The last term of (1b) is death rate $d_1 > 0$ of the predator population but it can also model other biological processes of which the loss rate is proportional to the population size similar to maintenance.

For a description of the state variables and the biological meaning of the parameters of the predator-prey model the reader is referred to Table 1.

Table 1: List of parameters and state variables and their reference values. We take the efficiency c_1 and death rate d_1 both proportional to the positive perturbation parameter ε . For numerical studies we take that parameter a_1 co-varies with b_1 via $a_1 = 5/3 b_1$, hence handling time is $3/5$ and the values for parameters $c = d = 1$ for the RM-model and $D = e_1 = 1$ for the MB-model. This is without loss of generality.

parameter	ref.values	Interpretation
t	$[0, \infty)$	Fast time variable
τ	$[0, \infty)$	Slow time variable
x_0	$[0, \infty)$	Nutrient density
x_1	$[0, \infty)$	Prey biomass density
x_2	$[0, \infty)$	Predator biomass density
x_r	$(0, \infty)$	Nutrient concentration in reservoir
a_1	$a_1 = 5/3 b_1$	Searching rate
b_1	3,4 or 8	Handling time \times searching rate
$c_1 = \varepsilon c$	$c = 1$	Conversion efficiency
$d_1 = \varepsilon d$	$d = 1$	Death rate
e_1	1	Conversion efficiency
$D_1 = \varepsilon D$	$D = 1$	Dilution rate
ε	$[0, 1]$	Perturbation parameter

The set of equations analysed extensively in the literature that form a model with slow-fast dynamics reads

$$\frac{dx_1}{dt} = f(x_1, x_2, \varepsilon) = x_1 \left(1 - x_1 - \frac{a_1 x_2}{1 + b_1 x_1} \right), \quad (2a)$$

$$\frac{dx_2}{dt} = \varepsilon g(x_1, x_2, \varepsilon) = \varepsilon x_2 \left(\frac{a_1 x_1}{1 + b_1 x_1} - 1 \right), \quad (2b)$$

with $x_i \in \mathbb{R}$, $i = 1, 2$. We introduced $c_1 = \varepsilon c$ and $d_1 = \varepsilon d$ and took for both parameters their reference value 1. The efficiency is again the ratio of the first term of (2b) and the last term on the right-hand sides of (2a) and is now equal to ε .

The functions $f : \mathbb{R}^3 \rightarrow \mathbb{R}$ and $g : \mathbb{R}^3 \rightarrow \mathbb{R}$ are of class smooth enough. The time-scale separation parameter ε is introduced in the model to implement trophic time diversification. For $\varepsilon \ll 1$ this is called a fast-slow system.

In the mathematical literature, factor ε is treated as a perturbation parameter, justified and described by the ratio between the linear death rate of the predator and the linear growth rate of the prey in [42, 16]. That is, only when the prey reproduce much faster than the predators and the predator is, in comparison, not so efficient, when the ratio ε becomes

a small parameter. For, the efficiency $c_1 = \varepsilon c$, where c is of order 1 (with a reference value 1) is proportional to the perturbation parameter ε .

The Holling type II hyperbolic relationship is derived by a time scale argument using a time budget modelling spend on searching for and handling of prey individuals by a predator individual. The ratio of these two terms is called the assimilation efficiency in ecology literature and the yield in the microbiology literature. When the units of both state variables equal then consequently $\varepsilon < 1$ means that there is a smaller than 100% biomass conversion, as is always the case in nature. We assume that the formed products during this conversion process, have no effects on other processes underlying model (2). In general, however, a very small conversion efficiency is not supported in the literature.

Observe that also the predator loss rate is multiplied by the same factor ε in order to facilitate coexistence. In other words when predators efficiency is low they also have to have a low loss rate in order to survive. Therefore the parameter ε affects two processes, mass conversion from prey biomass into predator biomass and the predator loss rate.

2.1 Existence and stability analysis of equilibria and limit cycles

In model (2) there are only three free parameters, namely a_1 , b_1 and ε which scales the efficiency and predator loss rate. The following stability analysis is classical for $\varepsilon > 0$ and therefore we recall some results regarding the dynamics of (2) and report some interesting results when $\varepsilon \rightarrow 0$ and $\varepsilon = 0$

The one-parameter bifurcation diagram with varying b_1 where $\varepsilon = 1$ and a_1 co-varies with b_1 via $a_1 = 5/3 b_1$, is shown in Fig. 1 for parameter b_1 as free parameter. The three relevant equilibria zero- E_0 , boundary- E_1 and interior equilibrium E_2 and the limit cycle L_2 are summarized in Table 2 and the bifurcation curves the transcritical bifurcation TC and Hopf bifurcation H in Table 3. In [19] it was proved that the coexistence equilibrium E_2 is globally stable and in [4] that the periodic solution is unique thus a globally unique stable limit cycle L_2 . The numerical bifurcation results show that the limit cycle for parameter values above the supercritical Hopf bifurcation is stable and that the minimum values become very small for large b_1 . This phenomenon is related to the “paradox of enrichment” [43], because extinction due to stochastic fluctuations is likely.

For the stability analysis of equilibria we need the Jacobian matrix evaluated at point (x_1, x_2) ([27]), which reads

$$\mathbf{J} = \begin{pmatrix} 1 - x_1 - \frac{a_1 x_2}{1+b_1 x_1} + x_1 \left(\frac{a_1 x_2 b_1}{(1+b_1 x_1)^2} - 1 \right) & -\frac{a_1 x_1}{1+b_1 x_1} \\ \varepsilon x_2 \left(\frac{a_1}{1+b_1 x_1} - \frac{a_1 x_1 b_1}{(1+b_1 x_1)^2} \right) & \varepsilon \left(\frac{a_1 x_1}{1+b_1 x_1} - 1 \right) \end{pmatrix}. \quad (3)$$

In E_0 the Jacobian matrix is

$$\mathbf{J}_0 = \begin{pmatrix} 1 & 0 \\ 0 & -\varepsilon \end{pmatrix}. \quad (4)$$

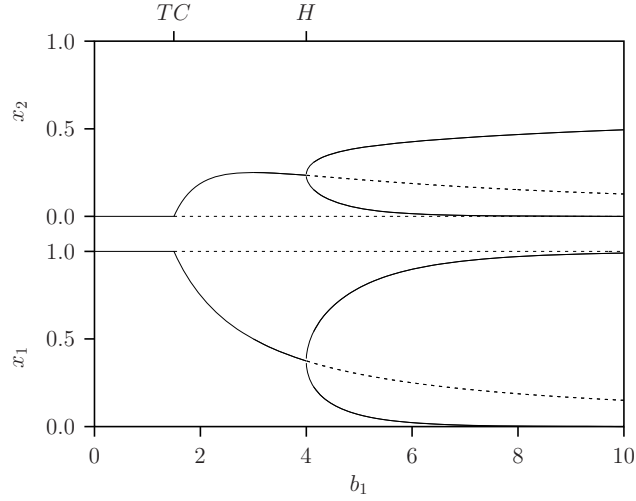


Figure 1: One-parameter bifurcation diagram for b_1 and $a_1 = 5/3 b_1$ of the RM-system (1) with $\varepsilon = 1$. The equilibria E_1 (below TC) and E_2 (between TC and H) as well as the maximum and minimum values for the limit cycle L_2 (above H) are shown. Note that the critical values where the bifurcations TC and H occur in this diagram are independent of ε since the expression for the real parts of the eigenvalues of the Jacobian matrix do not depend on ε .

Table 2: Equilibria of RM-model (2) and MB-model (54).

Equilibria	System composition
RM-model	
$E_0 = (0, 0)$	Extinction
$E_1 = (1, 0)$	Prey-only
$E_2 = (x_1^*, x_2^*) = (\frac{1}{a_1 - b_1}, \frac{a_1 - b_1 - 1}{(a_1 - b_1)^2})$	Prey-predator
MB-model	
$E_0 = (0, 0)$	Extinction
$E_1 = (1, 0)$	Prey-only
$E_2 = (x_1^*, x_2^*) = (\frac{1}{a_1 - b_1}, \frac{a_1 - b_1 - 1}{\varepsilon(a_1 - b_1)^2 + a_1 - b_1})$	Prey-predator

Table 3: Bifurcation curves for RM-model (2) and MB-model (54). Note that for RM-model the expression are independent of ε . The arrow indicates the transition of the steady states that occurs when the parameter crosses the bifurcation point.

Bifs.	$a_1(b_1, \varepsilon)$	b_1 ($a_1 = 5/3 b_1$)	Interpretation
RM-model			
TC	$a_1 = b_1 + 1$	1.5	$E_1 \rightarrow E_2$
H	$a_1 = \frac{b_1(b_1+1)}{b_1-1}$	4	$E_2 \rightarrow L_2$
MB-model			
TC	$a_1 = b_1 + 1$	1.5	$E_1 \rightarrow E_2$
H	$a_1 = \frac{2\varepsilon b_1^2 + 1 + \sqrt{4b_1^2\varepsilon(\varepsilon+1)+1}}{2\varepsilon(b_1-1)}$	$b_1 = \frac{4\varepsilon + \sqrt{16\varepsilon^2 + 15\varepsilon}}{(2\varepsilon)}$	$E_2 \rightarrow L_2$

160 The eigenvalues are the diagonal elements and the E_0 is always unstable. At the boundary
 161 equilibrium E_1 the Jacobian matrix reads

$$\mathbf{J}_1 = \begin{pmatrix} -1 & -\frac{a_1 - b_1 - 1}{1 + b_1} \\ 0 & \varepsilon \left(\frac{a_1 - b_1 - 1}{a_1} \right) \end{pmatrix}. \quad (5)$$

162 The eigenvalues are again the diagonal elements and E_1 is stable when $a_1 - b_1 - 1 < 0$ and
 163 unstable when $a_1 - b_1 - 1 > 0$. The equality gives the transcritical bifurcation TC where
 164 $b_1 = a_1 - 1$ or for the reference value $a_1 = 5/3 b_1$ we have $b_1 = 3/2$.

165 At the equilibrium E_2 the Jacobian matrix reduces to

$$\mathbf{J}_2 = \begin{pmatrix} \frac{a_1(b_1-1) - b_1(1+b_1)}{a_1((a_1-b_1))} & -1 \\ \varepsilon \left(\frac{a_1 - b_1 - 1}{a_1} \right) & 0 \end{pmatrix}. \quad (6)$$

The complex pair of eigenvalues $\lambda_{1,2}$ of the Jacobian matrix evaluated at the equilibrium E_2 read

$$\lambda_{1,2}(b_1, \varepsilon) = \mu(b_1) \pm i\omega(b_1, \varepsilon). \quad (7)$$

166 We calculated the following real $\mu \in \mathbb{R}$ and imaginary $\omega \in \mathbb{R}$ parts as functions of parameter
 167 ε and b_1 where $a_1 = 5/3 b_1$

$$\Delta(b_1, \varepsilon) = (\text{Tr } \mathbf{J}_2)^2 - 4 \det \mathbf{J}_2 = \frac{-144 + 72b_1 - 9b_1^2 - 60b_1\varepsilon + 40\varepsilon b_1^2}{25b_1^2}, \quad (8)$$

$$\mu(b_1, \varepsilon) = \frac{3(b_1 - 4)}{10b_1} \pm \frac{1 - \text{sgn } \Delta(b_1, \varepsilon)}{2} \sqrt{|\Delta(b_1, \varepsilon)|}, \quad (9)$$

$$\omega(b_1, \varepsilon) = \pm \frac{1 + \text{sgn } \Delta(b_1, \varepsilon)}{2} \sqrt{|\Delta(b_1, \varepsilon)|}. \quad (10)$$

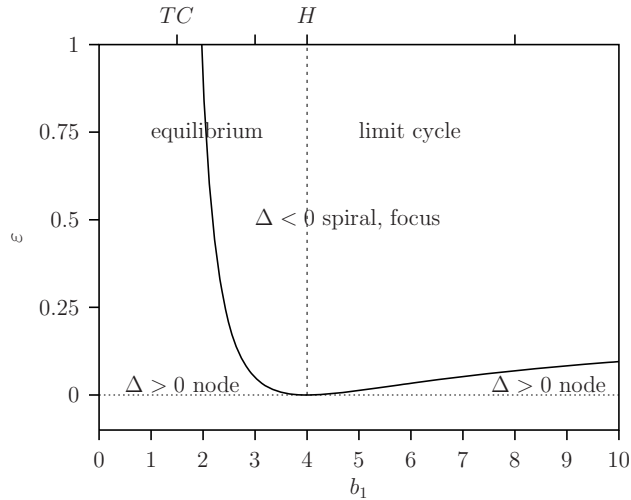


Figure 2: Focus bifurcation where $\Delta = 0$ curve for ε vs b_1 .

In Fig. 2 the curve where $\Delta(b_1, \varepsilon) = 0$ is plotted in the (b_1, ε) parameter space. This curve separates regions where the equilibrium is a node $\Delta > 0$ (two real eigenvalues) or a spiral or focus $\Delta < 0$ (two conjugated complex eigenvalues). At $\Delta = 0$ there are two equal real eigenvalues. From this figure we conclude that for $\varepsilon = 1$ and $b_1 = 3$ or $b_1 = 8$ the equilibria are foci while for $\varepsilon = 0.01$ the equilibria are nodes, stable and unstable, respectively.

The positions of the bifurcations TC and H are independent of the parameter ε . This is not true for the so called first Lyapunov coefficient ℓ^1 which determines whether the Hopf bifurcation is supercritical or subcritical, that is whether the emerging limit cycles are stable or unstable, respectively.

At the Hopf bifurcation with $b_1 = 4$ we have for $\varepsilon > 0$ a zero real part $\mu(4) = 0$ and the positive imaginary part equal to the determinant of the Jacobian matrix \mathbf{J}_2 : $\omega(4) = \sqrt{\det \mathbf{J}_2} = 1/2 \sqrt{\varepsilon}$, for the two conjugated complex eigenvalues. The square root of the ratio $\mu(b_1)/\omega(b_1)$ measures the amplitude of the limit cycle that emerge for the Hopf bifurcation for $b_1 > 4$. Evaluation of this ratio just above $b_1 = 4$ gives that the oscillatory dynamics for values is as with the Hopf bifurcation till the canard explosion occurs.

The derivative $d\mu/db_1(b_1)|_{b_1=4} = 3/40 > 0$ at the Hopf bifurcation equilibrium is positive and therefore the transversality condition for applying the normal form theorem [31, Theorem (3.3)] is satisfied. Using a similar procedure in Maple, [32] described in [31], the first Lyapunov coefficient ℓ^1 is evaluated as

$$\ell^1 = -\frac{16}{75} \frac{14\varepsilon + 1}{\varepsilon^{3/2}}. \quad (11)$$

Since ℓ^1 is negative for $\varepsilon > 0$, the Hopf bifurcation is supercritical. Note that for $\lim \varepsilon \rightarrow 0$ we have $\ell^1 \rightarrow -\infty$. That is, the first Lyapunov coefficient ℓ^1 becomes unbounded.

Furthermore, in the limiting case $\varepsilon = 0$ at the Hopf bifurcation where $b_1 = 4$ with $\mu(4) = 0$ we get together with $\omega(4) = 1/2 \sqrt{\varepsilon} = 0$ that this point becomes a degenerated bifurcation where both eigenvalues are zero as in a Bogdanov-Takens bifurcation point. Exploration of these facts can be done with a blow-up technique [8, 9] which is beyond the scope of this paper.

2.2 Phase-space analysis

In this section we discuss results in the phase-space of simulation in time. These results where in all simulations the same initial conditions are used, are shown in Fig. 3 and Fig. 4:

- Left panels of Fig. 3: for $b_1 = 3$, in the region between the transcritical TC and Hopf H bifurcation in Fig. 1 where equilibrium E_2 is stable,
- Fig. 4: for $b_1 = 4$ at the Hopf bifurcation,
- Right panels of Fig. 3: for $b_1 = 8$ above the Hopf bifurcation in Fig. 1 where equilibrium E_2 is unstable.

In the top panels of Fig. 3 and Fig. 4 the f-nullcline where $f(x_1, x_2, \varepsilon) = 0$: $x_2 = (1 - x_1)(1 + b_1 x_1)/a_1$ and the g-nullcline where $g(x_1, x_2, \varepsilon) = 0$: $x_1 = 1/(a_1 - b_1)$, are shown. Both are independent of ε . The graph of the f-nullcline is part of a parabola where it intersects the horizontal axis $x_2 = 0$ at $x_1 = 1$ and of the g-nullcline is just a vertical line through the equilibrium point E_2 .

2.2.1 Stable interior equilibrium

With $b_1 = 3$, see Fig. 3a with $\varepsilon = 1$ and Fig. 3c with $\varepsilon = 0.01$, the equilibrium E_2 is stable and there is convergence to the stable point.

For low $\varepsilon = 0.01$ value shown in Fig. 3c, initially after starting above the nullcline the solution goes rapidly to the vertical axis. There is almost no prey population and hence the predator population diminishes approximately exponential with rate $d_1 = 1$:

$$\frac{dx_2}{d\tau} = -x_2, \quad (12)$$

where differentiation is with respect to the slow time variable $\tau = \varepsilon t$. The solution crosses the critical point $x_2 = 1/a_1$ the intersection with the nullcline and leaves the vertical axis moving fast toward the stable part of the nullcline. Because this happens below the critical point (intersection of parabola and vertical axis) this phenomenon is called a *delayed bifurcation* which is explained in [42]. Eventually the system converges to the stable equilibrium E_2 given in Table 2.

2.2.2 Hopf interior equilibrium

The equilibrium E_2 , see Table 2, at the Hopf bifurcation H coincides with the top of the f-nullcline parabola

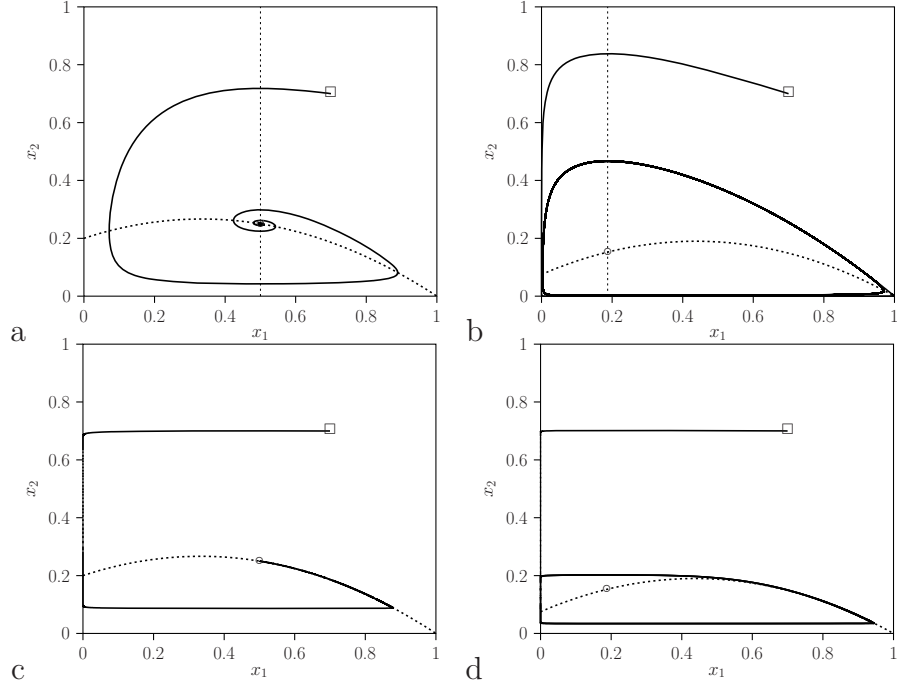


Figure 3: Phase-space analysis for system (2) describing the RM-model with $b_1 = 3$ (left panels) and $b_1 = 8$ (right panels) while $a_1 = 5/3 b_1$. Top panels (a,b): $\varepsilon = 1$ and bottom panels (c,d): $\varepsilon = 0.01$. (a): Spiral stable equilibrium E_2 , (b): stable limit cycle L_2 , (c): node stable equilibrium E_2 and (d): stable limit cycle L_2 .

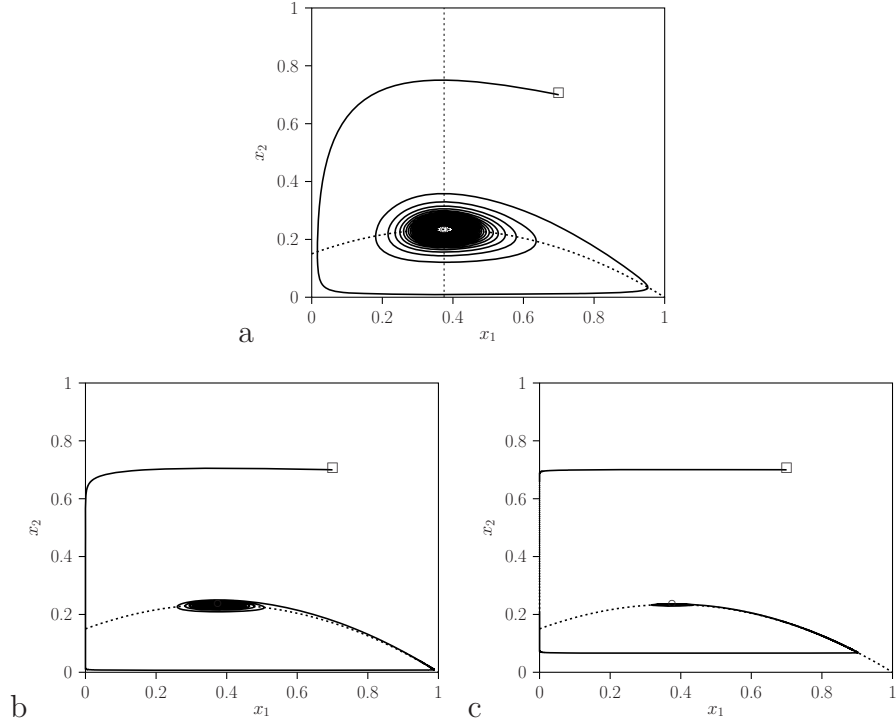


Figure 4: Phase-space analysis for system (2) describing the RM-model, $b_1 = 4$ and $a_1 = 5/3 b_1$, that is at the Hopf bifurcation point for three different values of ε : $\varepsilon = 1$ (a), $\varepsilon = 0.1$ (b) and $\varepsilon = 0.01$ (c).

$$(\bar{x}_1, \bar{x}_2)_T = \left(\frac{b_1 - 1}{2b_1}, \frac{(b_1 + 1)^2}{4a_1 b_1} \right). \quad (13)$$

At the Hopf point we have the equilibrium E_2

$$(x_1^*, x_2^*)_H = (\bar{x}_1, \bar{x}_2)_T = \left(\frac{3}{8}, \frac{15}{64} \right). \quad (14)$$

The simulation results for system (2) are shown in Fig. 4. These results show that the solution finally converges very slowly to this, sometimes called a weakly attracting, equilibrium (14) at the top of the f-nullcline denoted by (13).

2.2.3 Unstable interior equilibrium

With $b_1 = 8$, see Fig. 3b,d equilibrium E_2 is unstable and there is no convergence to E_2 but to a stable limit cycle L_2 .

For positive $\varepsilon = 0.01$ in Fig. 3d initially the dynamics is similar to that for the stable case shown in Fig. 3c. The dynamics on the unique stable limit cycle L_2 consists of four

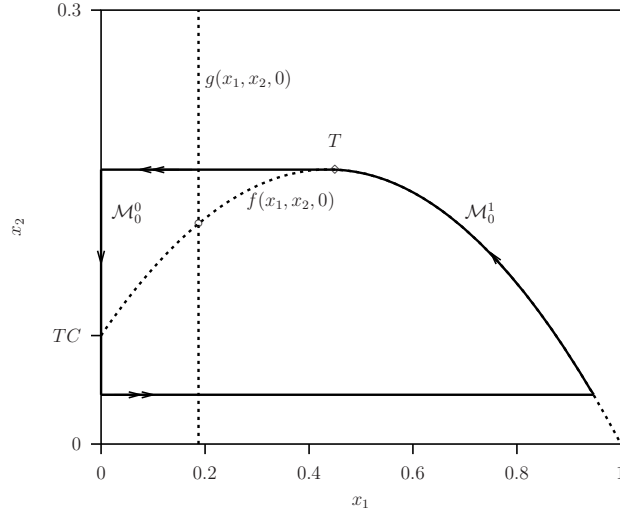


Figure 5: Fast (double arrow) and slow (single arrow) dynamics for system (2) describing the RM-model with $b_1 = 8$ where for $\lim \varepsilon \rightarrow 0$ the concatenated trajectories are the degenerated phase curves. The f-nullcline (parabola) and g-nullcline (vertical line through equilibrium) are shown. Point T is top of parabola given in (13) and TC is intersection point of f-nullcline and vertical axis.

concatenated episodes. Two parts of the trajectory where the predator population changes slowly and two parts of the trajectory where the predator population is almost constant and the prey population changes fast (the almost horizontal parts of the solution orbit).

2.2.4 Degenerate phase curves

With $b_1 > 4$ the limits of the limit cycles L_2 , the periodic *relaxation oscillations*, for $\lim \varepsilon \rightarrow 0$ are called *degenerated phase curves* shown in Fig. 5, see [14] It consists of four concatenated episodes (families of periodic sets). On two parts of the trajectory the dynamics is slow (single arrow): one along the vertical axis where the predator population decreases slowly and the other are along parts of the parabolic f-nullcline where the prey population decreases while the predator population increases slowly. On the other two parts of the trajectory the prey changes fast (double arrows) and the predator is constant: one from point T toward the vertical axis and one from this vertical axis to the point on the parabolic f-nullcline. This type of dynamics is discussed intensively in the ecological literature, we mention [42, 11] and references therein. These two episodes are connected by two fast episodes along the horizontal lines where the prey population size increases or decreases fast while the predator population is constant.

Starting slowly on the vertical axis above the f-nullcline, during the first episode, the solution orbit crosses the critical point TC and leaves this axis fast horizontally toward the parabola. Then it continues, during the second episode, slowly and during the third episode again along the parabola passing the top of the parabola point T given in (13).

252 Note that since $b_1 > 4$ the equilibrium E_2 indicated by the open circle in Fig. 5 on the
 253 f-nullcline, does not coincide with this non-hyperbolic point T . After crossing this point
 254 the solution orbit, during the forth episode, moves vastly horizontally toward the vertical
 255 axis again above the f-nullcline, and so on.

256 Note that the dynamics of the degenerate phase curves shown in Fig. 5 are indeed close
 257 to this for the RM-model in Fig. 3d where $b_1 = 8$ in both cases. However for the Hopf
 258 bifurcation $b_1 = 4$ case the resulting dynamics for small $\varepsilon \ll 1$ does not look like that of
 259 Fig. 5 and more importantly also not for b_1 slightly above the Hopf bifurcation. Therefore
 260 we focus in the next sections on the dynamics for parameter values where the unstable
 261 equilibrium E_2 is just above the Hopf bifurcation value.

262 3 Singular perturbation problem

263 In this section the singular perturbation technique is used to analyse the singular pertur-
 264 bation problem where $\varepsilon = 0$ in the RM-model (2). We will also analyse the quasi-steady
 265 state solution or the relaxation oscillation in detail. The reader is referred to [18, 21, 22]
 266 for introductions into perturbation analysis.

267 3.1 Heuristic introduction

268 We start with a short overview of singular perturbation techniques. Singular perturbation
 269 theory deals with systems of the *original* form (2) where $\varepsilon > 0$. When $\varepsilon \ll 1$ the system
 270 is a fast-slow system.

271 With $\varepsilon = 0$ we have the *fast system* also called the *layer system*:

$$\frac{dx_1}{dt} = f(x_1, x_2(0), 0) = x_1(1 - x_1 - \frac{a_1 x_2(0)}{1 + b_1 x_1}) , \quad (15a)$$

$$\frac{dx_2}{dt} = 0 . \quad (15b)$$

272 The predator populations remains constant hence the trajectories are the horizontal lines
 273 in Fig. 5.

274 With a change of time-scale, where $\tau = \varepsilon t$, we call the resulting system the *slow system*:

$$\varepsilon \frac{dx_1}{d\tau} = f(x_1, x_2, \varepsilon) , \quad (16a)$$

$$\varepsilon \frac{dx_2}{d\tau} = \varepsilon g(x_1, x_2, \varepsilon) . \quad (16b)$$

275 After substitution of $\varepsilon = 0$ we get

$$0 = f(x_1, x_2, 0) , \quad (17a)$$

$$\frac{dx_2}{d\tau} = g(x_1, x_2, 0) = x_2 \left(\frac{a_1 x_1}{1 + b_1 x_1} - 1 \right) . \quad (17b)$$

This differential algebraic equation (DAE) is called the *reduced system*. The trajectory is either part of the vertical axis where $x_2 = 0$ or part on the parabola, the other f-nullcline of the original system (2) in Fig. 5. However, in the fast-slow context these are the sets of equilibria of the fast layer-system (15) and then they are called *critical manifolds* where x_1 is acting as a parameter.

These heuristic results suggest the following approach for dealing with the two different time scales. The first step consists in setting $\varepsilon = 0$ which gives the set of fast equilibria of the fast system (15) yielding the algebraic equation (17a). This is the critical manifold which is the set of equilibria either at the vertical axis or the parabola where $f(x_1, x_2, 0) = 0$.

From the results presented below in this section the parabolic critical manifold has two branches, one stable on the right-hand side (solid curve) and one unstable on the left-hand side (dashed curve) of point T in Fig. 5.

With good hypothesis (see below for the details), on the part of the parabola, $f(x_1, x_2, 0) = 0$ is equivalent to $x_1 = p(x_2)$ and we can substitute x_1 by $p(x_2)$ in equation (17b). The result is the slow or reduced system

$$0 = f(p(x_2), x_2, 0) , \quad \frac{dx_2}{d\tau} = g(p(x_2), x_2) . \quad (18)$$

The differentiation is with respect to τ and the smooth functions f and g are defined in (2). Then the slow system becomes

$$\frac{dx_2}{d\tau} = x_2 \left(\frac{(a_1 - b_1)p(x_2) - 1}{b_1 p(x_2) + 1} \right) , \quad x_1 = p(x_2) = \frac{1}{2b_1} (b_1 - 1 \pm \sqrt{(b_1 + 1)^2 - 4a_1 b_1 x_2}) . \quad (19)$$

An alternative method is to use instead of $x_1 = p(x_2)$ of which the dynamics is described by the solution of (19), the inverse function $x_2 = q(x_1)$ also derived from (17a). This gives the relationship

$$x_2 = q(x_1) = \frac{1}{a_1} (1 - x_1)(1 + b_1 x_1) , \quad (20)$$

and using (17b) the differential equation

$$\frac{dx_2}{d\tau} = g(x_1, q(x_1)) = \frac{dq}{dx_1} \frac{dx_1}{d\tau} ,$$

298 and we get formally

$$\frac{dx_1}{d\tau} = \frac{q(x_1)(a_1x_1 - (1 + b_1x_1))}{(1 + b_1x_1) dq/dx_1}, \quad \frac{dq}{dx_1} = \frac{1}{a_1} (b_1(1 - 2x_1) - 1). \quad (21)$$

299 Note that this expression is zero at point T given in (13). Hence the denominator of model
 300 (21) at that point T is zero. When the numerator is unequal zero, this means that the rate
 301 of change becomes unbounded at T which is a singular point of model (21). Only when in
 302 the special case b_1 is the Hopf bifurcation parameter value, point T is a limit point where
 303 the numerator is also zero. This is studied in the Appendix B.

304 3.2 Geometric singular perturbation techniques

305 We discuss the singular perturbation problem outlined in the previous section for the case
 306 where ε is not zero but small and positive: $0 < \varepsilon \ll 1$. Here we follow the geometric
 307 singular perturbation techniques.

308 Let us consider system (2) again. For $\varepsilon = 0$ the f-nullclines, the set $\{(x_1, x_2) | f(x_1, x_2, 0) =$
 309 $0, x_1 \geq 0, x_2 \geq 0\}$ consist of two types of critical manifolds, see Fig. 5

$$\mathcal{M}_0^0 = \{(x_1, x_2) | x_1 = 0, x_2 \geq 0\} \quad (22a)$$

$$\mathcal{M}_1^0 = \{(x_1, x_2) | x_2 = \frac{1}{a_1}(1 - x_1)(1 + b_1x_1), x_1, x_2 \geq 0\}. \quad (22b)$$

310 They form a set of equilibria of the fast system system (15). In the previous section we
 311 studied the dynamics for $\varepsilon = 0$ and now we will consider $0 < \varepsilon \ll 1$.

312 To that end, let us remind the statement of Fenichel's theorem. We consider differential
 313 system of the form:

$$\frac{dX}{dt} = F(X, Y, \varepsilon), \quad (23a)$$

$$\frac{dY}{dt} = \varepsilon G(X, Y, \varepsilon), \quad (23b)$$

$$\frac{d\varepsilon}{dt} = 0, \quad (23c)$$

314 where F and G are sufficiently smooth. We assume that the set $F(X, Y, 0) = 0$ can locally
 315 be written as $X = H(Y)$, which defines a critical manifold. If, for all Y in a given compact
 316 set \mathcal{D} , all the eigenvalues of $\frac{DF}{DX}(H(Y), Y, 0)$ have a non-vanishing real part, then the critical
 317 manifold is said *normally hyperbolic*. In this case, there exists ε_0 and a map p defined on
 318 $\mathcal{D} \times [0, \varepsilon_0[$ such that:

319 i) $H(Y) = p(Y, 0)$;

ii) the graph of p is invariant under the flow associated to the original differential system (23);

iii) the graph of p is tangent to the central space associated to the linearisation of the system at $(H(Y), Y, 0)$.

As a consequence, both critical manifolds \mathcal{M}_0^0 and \mathcal{M}_0^1 are normally hyperbolic and there exists ε_0 such that for $0 < \varepsilon < \varepsilon_0$, there are locally invariant manifolds $\mathcal{M}_\varepsilon^0$ and $\mathcal{M}_\varepsilon^1$ except in the neighborhood of point T $(x_1, x_2) = (\bar{x}_1, \bar{x}_2)$ and in the neighborhood of the intersection between \mathcal{M}_0^0 and \mathcal{M}_0^1 on the vertical axis. Indeed, at those points, the derivative of the fast part vanishes, which contradicts the assumptions of the theorem statement.

Using its invariance, the perturbed manifold $\mathcal{M}_\varepsilon^1$ can be approximated by asymptotic expansions in ε . It can be described as a graph

$$\{(x_1, x_2) | x_2 = q(x_1, \varepsilon), x_1 \geq 0, x_2 \geq 0\} . \quad (24)$$

This manifold is invariant when the following equality holds

$$\frac{dx_2}{dt} = \frac{dx_2}{dx_1} \frac{dx_1}{dt} = \frac{dq(x_1, \varepsilon)}{dx_1} \frac{dx_1}{dt} , \quad (25)$$

yields with equation (23) and $x_2 = q(x_1, \varepsilon)$:

$$\frac{\partial q(x_1, \varepsilon)}{\partial x_1} \frac{dx_1}{dt} = \varepsilon q(x_1, \varepsilon) \left(\frac{x_1(a_1 - b_1) - 1}{1 + b_1 x_1} \right) . \quad (26)$$

Then (23) gives with $x_2 = q(x_1, \varepsilon)$ the invariance condition

$$\frac{\partial q(x_1, \varepsilon)}{\partial x_1} x_1 \left(1 - x_1 - \frac{a_1 q(x_1, \varepsilon)}{1 + b_1 x_1} \right) = \varepsilon q(x_1, \varepsilon) \left(\frac{x_1(a_1 - b_1) - 1}{1 + b_1 x_1} \right) , \quad (27)$$

or using $1 + b_1 x_1 > 0$

$$\frac{\partial q(x_1, \varepsilon)}{\partial x_1} x_1 \left((1 - x_1)(1 + b_1 x_1) - a_1 q(x_1, \varepsilon) \right) = \varepsilon q(x_1, \varepsilon) (x_1(a_1 - b_1) - 1) . \quad (28)$$

3.2.1 Asymptotic expansion

The following asymptotic expansion in ε is introduced:

$$q(x_1, \varepsilon) = q_0(x_1) + \varepsilon q_1(x_1) + \varepsilon^2 q_2(x_1) + \dots , \quad (29)$$

338 hence

$$\frac{\partial q}{\partial x_1} = \frac{dq_0}{dx_1} + \varepsilon \frac{dq_1}{dx_1} + \varepsilon^2 \frac{dq_2}{dx_1} + \dots \quad (30)$$

339 Substitution into (28) gives

$$\begin{aligned} & \left(\frac{dq_0}{dx_1} + \varepsilon \frac{dq_1}{dx_1} + \varepsilon^2 \frac{dq_2}{dx_1} + \dots \right) x_1 \left((1 - x_1)(1 + b_1 x_1) - a_1(q_0(x_1) + \varepsilon q_1(x_1) + \varepsilon^2 q_2(x_1) + \dots) \right) \\ &= \left(\varepsilon(q_0(x_1) + \varepsilon q_1(x_1) + \dots) \right) (x_1(a_1 - b_1) - 1) . \end{aligned} \quad (31)$$

340 Gathering orders of ε results for $\mathcal{O}(1)$ and assuming $x_1 > 0$ in:

$$q_0(x_1) = \frac{(1 - x_1)(1 + b_1 x_1)}{a_1} , \quad \frac{dq_0}{dx_1} = \frac{b_1 - 1 - 2x_1 b_1}{a_1} . \quad (32)$$

341 At $b_1 = 4$ we have $x_1 = (b_1 - 1)/(2b_1)$ and hence $dq_0/dx_1 = 0$.

342 For $\mathcal{O}(\varepsilon)$ and using an updated form of (28)

$$\frac{\partial q(x_1, \varepsilon)}{\partial x_1} x_1 a_1 (q_0 - q(x_1, \varepsilon)) = \varepsilon q(x_1, \varepsilon) (x_1(a_1 - b_1) - 1) , \quad (33)$$

343 gives

$$q_1(x_1) = q_0(x_1) \frac{(x_1(a_1 - b_1) - 1)}{-a_1 x_1 \frac{dq_0}{dx_1}} . \quad (34)$$

344 At $b_1 = 4$ the numerator and denominator are both zero. we have $x_1 = (b_1 - 1)/(2b_1)$ and
345 $dq_0/dx_1 = 0$ but also since it is a equilibrium $x_1(a_1 - b_1) - 1 = 0$.

346 For $\mathcal{O}(\varepsilon^2)$ in (33) gives

$$q_2(x_1) = q_1(x_1) \frac{\frac{dq_1}{dx_1} x_1 a_1 + x_1(a_1 - b_1) - 1}{-a_1 x_1 \frac{dq_0}{dx_1}} . \quad (35)$$

347 At point T we have $x_1 = \bar{x}_1 = (b_1 - 1)/(2b_1)$ where $dq_0/dx_1 = 0$. Consequently, at
348 that point the denominator in the expression for $q_i(\bar{x}_1), i > 0$ is zero. Therefore the
349 coefficients $q_i(\bar{x}_1), i > 0$ are unbounded when the numerator is not equal zero. Only when
350 the parameter $b_1 = 4$ is at the Hopf bifurcation the numerator is zero and the coefficients
351 $q_i(\bar{x}_1)$ remain finite.

3.2.2 Asymptotic expansion in phase space

The expression for q_0 describes the critical manifold \mathcal{M}_0^1 . This expression is the inverse (when it exists) of $p(x_2)$ in (19). The voluminous expressions for the higher order q_i , $i > 1$ coefficients obtained by equating the $\mathcal{O}(\varepsilon^i)$ terms on the left- and right-hand side of the invariance condition (28), are not given here but are available using Maple, [32]. This yields the approximation of the perturbed slow manifold $\mathcal{M}_\varepsilon^1$

For $\varepsilon = 0$ the limit (16b) prescribes the singular slow flow on \mathcal{M}_0^1 with $\tilde{x}_2 = q_0(\tilde{x}_1)$ given by (32)

$$\frac{d\tilde{x}_1}{dt} = \tilde{x}_1 \left(1 - x_1 - \frac{a_1 q_0(\tilde{x}_1)}{1 + b_1 \tilde{x}_1} \right). \quad (36)$$

For sufficiently small non-zero $\varepsilon \ll 1$ the flow on the perturbed slow manifold $\mathcal{M}_\varepsilon^1$ can be approximated by inserting $\tilde{x}_2 = q(\tilde{x}_1, \varepsilon)$ with $q(\tilde{x}_1, \varepsilon)$ given by (29). In order to simulate the model we solve

$$\frac{d\tilde{x}_1}{dt} = \tilde{x}_1 \left(1 - \tilde{x}_1 - \frac{a_1 q(\tilde{x}_1, \varepsilon)}{1 + b_1 \tilde{x}_1} \right), \quad (37)$$

with properly chosen the initial values.

The results are shown in Fig. 6 for $b_1 = 3$, where the equilibrium E_2 is stable. They show that in this case the solution of the original model on $\mathcal{M}_\varepsilon^1$ is already well approximated by the second order approximation when $\varepsilon = 0.1$.

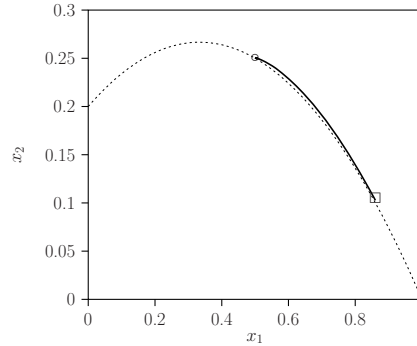


Figure 6: Results for the original system (2) (solid) describing the RM-model (29) with $b_1 = 3$ where $a_1 = 5/3 b_1$ and initial conditions $x_1 = 0.86038$ and $x_2(0) = 0.102646$.

In Fig. 7a and Fig. 7b the graph of the function $q(x_1, \varepsilon)$ is shown for $b_1 = 3$ and $b_1 = 8$, respectively. These results show that the asymptotic expansion for $\varepsilon > 0$ is only locally a good approximation for $\mathcal{M}_\varepsilon^1$ but fails at the top of the parabola point T .

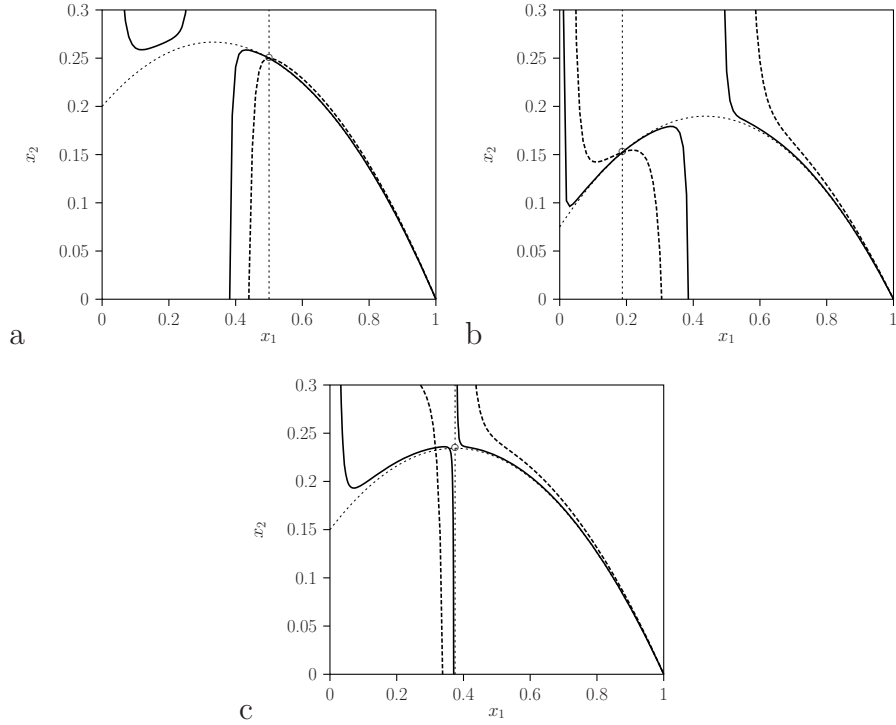


Figure 7: Second-order approximation of $\mathcal{M}_\varepsilon^1$ results with (a): $b_1 = 3$ (b): $b_1 = 8$ and (c): $b_1 = 4$ where $a_1 = 5/3 b_1$ for the RM-model (29). Solid: with $\varepsilon = 0.01$. Dotted with $\varepsilon = 0.1$.

At the Hopf bifurcation In Fig. 7c the graph of the function $q(x_1, \varepsilon)$ is shown for $b_1 = 4$. While the solution converges to the neutral stable equilibrium E_2 where the rate of convergence becomes slower when approaching the non-hyperbolic point (see also Fig. 4b,c) the asymptotic expansion explodes and there is discontinuity at $x_1 = x_1^* = \bar{x}_1$:

$$\lim_{x_1 \downarrow \bar{x}_1} q(x_1, \varepsilon) = \infty \quad \text{and} \quad \lim_{x_1 \uparrow \bar{x}_1} q(x_1, \varepsilon) = -\infty. \quad (38)$$

In the next section we extend the asymptotic expansion in ε by varying parameter b_1 in addition to ε in order to repair this unwanted property.

3.3 Canard explosion

In this section we analyse the Canard dynamics that occurs for b_1 values just above the Hopf bifurcation at $b_1 = 4$ similar to the analysis performed in [2]. Other papers on canards are [10, 6, 8, 11, 2]. We will expand the asymptotic expansion discussed in the previous section where the equilibrium point is unstable and the system itself shows oscillatory behaviour, a stable limit cycle.

383 We start with an exploration of this oscillatory behaviour for b_1 values just above the
 384 Hopf bifurcation by simulation of the full model in time for small ε values. In order to
 385 study the dynamics for small ε in more detail we re-analyse the continuation as in Fig. 1
 386 where $\varepsilon = 1$ in the region close to the Hopf bifurcation at $b_1 = 4$. The results are shown
 387 for $\varepsilon = 0.01$ in Fig. 8.

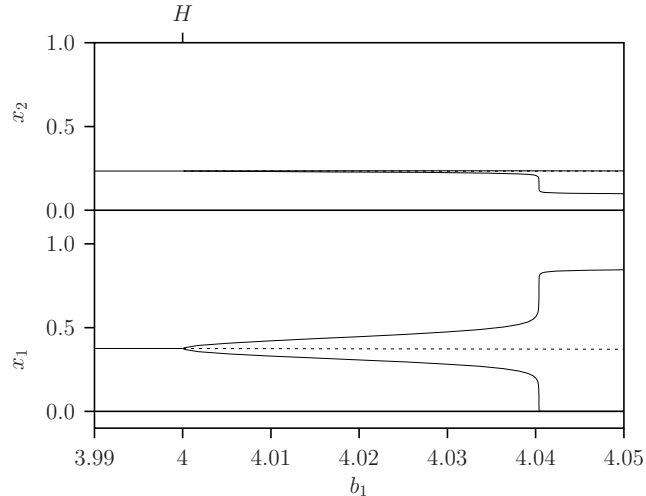


Figure 8: One-parameter bifurcation diagram for b_1 and $a_1 = 5/3 b_1$ of the RM-system (1) with $\varepsilon = 0.01$.

388 Unexpectedly the amplitude of the limit cycle increases sharply when b_1 passes a value
 389 just above $b_1 = 4.04$. In Fig. 9 parameter ε is varied continuously for a number values of
 390 b_1 just above the Hopf bifurcation point. Using (8) these results support the analytical
 391 expression for the amplitude of the unique stable limit cycles emerging from the Hopf
 392 bifurcation for small ε values being: $\sqrt{\mu(b_1)/\omega(b_1)}$.

393 The continuation of the curves calculated with AUTO [7] failed for small ε . This is due
 394 to the part of the cycle close to the vertical axis where x_1 is small, see Fig. 3bd. In order
 395 to avoid this dynamics we study now an augmented system

$$\frac{dx_1}{dt} = \delta + f(x_1, x_2, \varepsilon) = \delta + x_1 \left(1 - x_1 - \frac{a_1 x_2}{1 + b_1 x_1} \right), \quad (39a)$$

$$\frac{dx_2}{dt} = \varepsilon g(x_1, x_2, \varepsilon) = \varepsilon x_2 \left(\frac{a_1 x_1}{1 + b_1 x_1} - 1 \right), \quad (39b)$$

396 where δ is a small allochthonous input rate of the prey population. Addition of this extra
 397 term removes the transcritical bifurcation at $x_2 = 1/a_1$ because it is structurally unstable
 398 with respect to such a perturbation. Fig. 10 is a similar diagram as Fig. 9 where $\delta = 0.0001$
 399 instead of $\delta = 0$. Note that the Hopf bifurcation occurs at values slightly different from
 400 $b_1 = 4$, namely at $b_1 = 4.000711364$ and this is taken into account in what follows. The

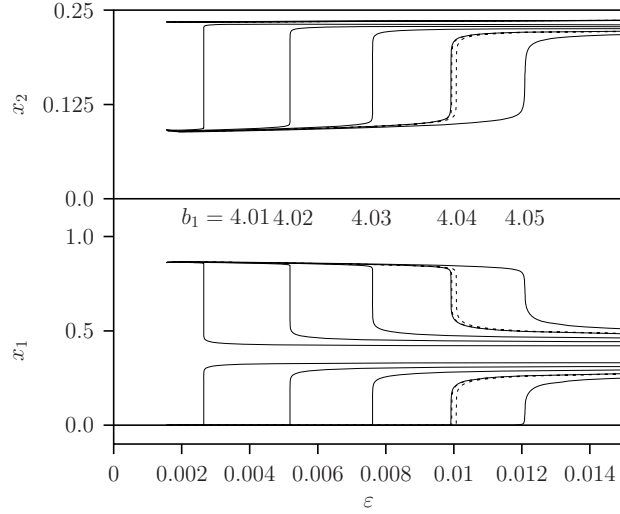


Figure 9: One-parameter bifurcation diagram for ε with various $b_1 = 4.01, 4.02, 4.03, 4.04, 4.0401, 4.0407, 4.05$ values where $a_1 = 5/3 b_1$ of the RM-system (1). For $b_1 > 4$ the minimum and minimum populations values during the stable limit cycle are shown. Also the two dashed curves are shown for $b_1 = 4.0409$ and 4.04061 . Between these two values the explosion occurs at $\varepsilon = 0.01$ see also Fig. 8. The curves terminate for low ε values. This is due to numerical problems of the parameter continuation for these low values. Theory predicts that these curves of maximums and minimums are continuing almost horizontally.

results in Fig. 10 imply that continuation is possible toward very low ε values. The results show that the canard is a robust and smooth phenomenon that occurs for stable limit cycles. When $\varepsilon \downarrow 0$ the canard explosion point converges to the point T .

In Fig. 11 the shape of the limit cycles is shown for two values of b_1 just below and above the sudden changes: $b_1 = 4.04019$ and $b_1 = 4.04061$ where $\varepsilon = 0.01$. These results show how the unique stable limit cycle changes shape very abruptly at $b_1 \approx 4.0403$ where b_1 is varied keeping ε fixed: the canard explosion. In Fig. 12 the shape of the limit cycles is shown for four values: $\varepsilon = 0.008, 0.009$, big stable limit cycles and $\varepsilon = 0.01, 0.011$, small stable limit cycles with fixed $b_1 = 4.0403$, the value calculated with the extended asymptotic expansion technique. These results show the dynamics with ε values above the canard explosion at approximately $\varepsilon = 0.01$, are limit cycles with small amplitudes consisting of two concatenated slow (close to the critical manifold and just above the parabola) and fast (almost horizontal part of the trajectory below the parabola). Below the canard explosion the limit cycles with large amplitudes consist of four episodes, two slow (close to the critical manifold, one just above the parabola and one close to the vertical axis) and two fast (almost horizontal, one leaving close from point T and one leaving the vertical axis and landing close to the parabola).

Careful examination indicates that there is one point where the trajectories for the four ε values intersect. Starting at that point and changing ε gives the unique stable limit

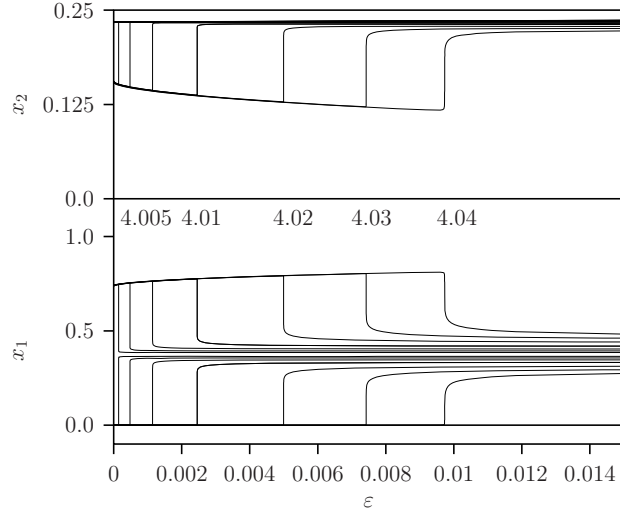


Figure 10: One-parameter bifurcation diagram for ε with various $b_1 = 4.00125, 4.0025, 4.005, 4.01, 4.02, 4.03, 4.04$ values where $a_1 = 5/3 b_1$ of system (39) with prey input rate $\delta = 0.0001$. The parameter continuation is here successful to very small values of ε .

cycles calculated and this shows that these curves change smoothly, only the sensitivity of the shape of the cycles is very large at the explosion point.

3.3.1 Asymptotic expansion and canard explosion

Following [13] we repeat the extended asymptotic expansion in ε technique introduced in (29) now near the Hopf bifurcation point. To that end the expansion is not only taken for the function $x_2 = q(x_1, \varepsilon)$ evaluated at $q_0(x_1)$ (see (32)) but also in the bifurcation parameter $b_1 = b_1(\varepsilon)$ and consequently $a_1(\varepsilon) = 5/3 b_1(\varepsilon)$ evaluated at the Hopf bifurcation point $b_{10} = 4$ with $a_{01} = 20/3$. This comes with more freedom which leads to an extra criterion: the singularity of the approximation at point T is removed. This function is now denoted as $r(x_1, \varepsilon)$ and the expansion is evaluated at $r(x_1 = \bar{x}_1, \varepsilon = 0)$. When $b_1 = b_{10}$ we have $r(\bar{x}_1, \varepsilon) = q(\bar{x}_1, \varepsilon)$.

Similar to the invariance condition of the perturbed slow manifold $\mathcal{M}_\varepsilon^1$ we derive now the adapted equation that replaces (28) where we substitute $a_1(\varepsilon) = 5/3 b_1(\varepsilon)$:

$$\frac{\partial r}{\partial x_1} x_1 \left((1 - x_1)(1 + b_1(\varepsilon)x_1) - 5/3 b_1(\varepsilon)r(x_1, \varepsilon) \right) = \varepsilon r(x_1, \varepsilon) (2/3 x_1 b_1(\varepsilon) - 1). \quad (40)$$

The following extended asymptotic expansion in ε for $r(x_1, \varepsilon)$ is introduced as follows:

$$x_2 = r(x_1, \varepsilon) = r_0(x_1) + \varepsilon r_1(x_1) + \varepsilon^2 r_2(x_1) + \dots, \quad (41)$$

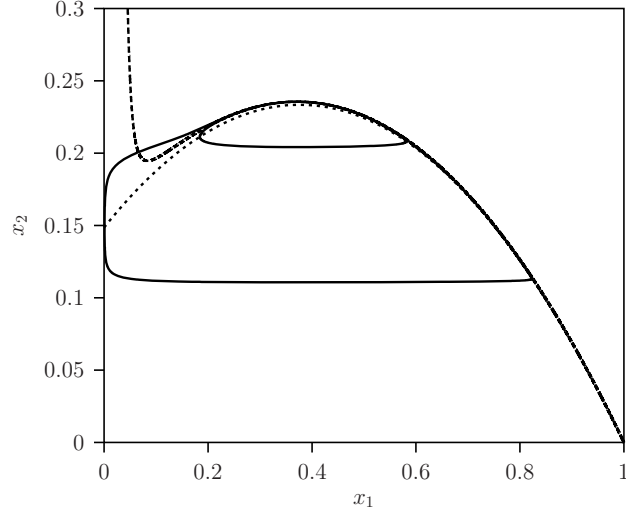


Figure 11: Phase-space diagram with $\varepsilon = 0.01$. Solid lines: stable limit cycle for two values of $b_1 = 4.04019$ (small cycle) and $b_1 = 4.04061$ (big cycle) while $a_1 = 5/3 b_1$ of the RM-system (1). Dashed line: extended asymptotic expansion $r(x_1, \varepsilon)$ of $\mathcal{M}_\varepsilon^1$ (41) where $b_1 = 4.0403$.

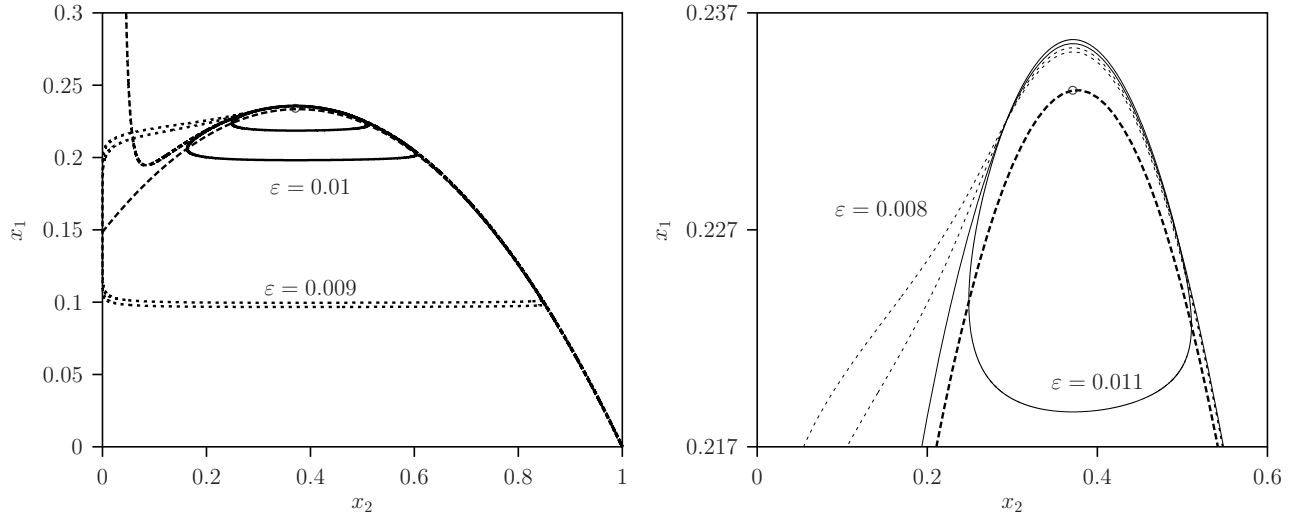


Figure 12: Phase-space diagram with $\varepsilon = 0.008, 0.009, 0.01, 0.011$. Solid lines: stable limit cycle for two values $\varepsilon = 0.008, 0.009$ (big cycle) and two values $\varepsilon = 0.01, 0.011$ (small cycle) of the RM-system (1). Dashed line: extended asymptotic expansion $r(x_1, \varepsilon)$ of $\mathcal{M}_\varepsilon^1$ (41) where $b_1 = 4.0403$.

434 and

$$\frac{\partial r}{\partial x_1} = \frac{dr_0}{dx_1} + \varepsilon \frac{dr_1}{dx_1} + \varepsilon^2 \frac{dr_2}{dx_1} + \dots, \quad (42)$$

435 whereby $b_1(\varepsilon)$ is given by

$$b_1(\varepsilon) = b_{10} + \varepsilon b_{11} + \varepsilon^2 b_{12} + \varepsilon^3 b_{13} + \varepsilon^4 b_{14} \dots, \quad (43)$$

436 where r_j and b_{1j} , $j = 1 \dots$ are independent of ε and are described by the invariance
437 condition (40) by equality order by order of powers of ε of this condition. Equating $\mathcal{O}(1)$
438 terms yields:

$$r_0 = \frac{(1 - x_1)(1 + b_{10}x_1)}{5/3 b_{10}}. \quad (44)$$

439 With $b_{10} = 4$ this gives the zero order approximation of $\mathcal{M}_\varepsilon^1$ equal to \mathcal{M}_0^1 . Using (44)
440 and substitution of (41), (42) and (43) in (40) and equating the resulting first order $\mathcal{O}(\varepsilon)$
441 terms, yields:

$$r_1(x_1) = \frac{3(1 - x_1)(1 - b_{10} + 2x_1 b_{10})b_{11}x_1 b_{10} - x_1 b_{10}^2 - 3b_{10} + 2x_1^2 b_{10}^3}{5b_{10}^2(1 + 2x_1 b_{10} - b_{10})x_1}. \quad (45)$$

442 It appears that the terms with b_{11} , namely $3x_1 b_{11}(b_{10} - 1 - 2x_1 b_{10}) = 0$, are already
443 eliminated when they are evaluated at the Hopf bifurcation support point with $b_{10} = 4$ and
444 $a_{10} = 20/3$ at the equilibrium E_2 with $x_1 = \bar{x}_1 = x_1^* = 1/(a_{10} - b_{10})$. At that point both
445 the numerator and the denominator are zero but $\lim_{x_1 \downarrow \bar{x}_1} r_1(x_1) = \lim_{x_1 \uparrow \bar{x}_1} r_1(x_1)$ and this
446 shows that function $r_1(x_1)$ is continuous for all b_{11} .

447 From this point a recursive procedure can be followed. One by one, r_i , $i \geq 2$ is
448 determined by taking the i^{th} order term in the invariance condition (40) equal to zero and
449 thereafter the term $b_{1(i-1)}^{\text{th}}$ by the condition that this term is continuous at $x_1 = \bar{x}_1 =$
450 $(b_{10} - 1)/(2b_{10})$. This means that the free parameter is chosen such that the singularity is
451 removed. The requirement that the sum of second order terms is zero gives

$$r_2 = (1 - x_1) \frac{(-288x_1^4 + 108x_1^3)b_{12} + (72x_1^4 - 27x_1^3)b_{11}^2 + (96x_1^3 + 84x_1^2)b_{11} + 256x_1^3 - 128x_1^2 - 112x_1 - 16}{960x_1^3(8x_1 - 3)}. \quad (46)$$

452 At the support point T being the Hopf bifurcation point with $b_{10} = 4$ and $x_1 = \bar{x}_1$ given by
453 (14) we have $(-288x_1^4 + 108x_1^3)b_{12} = 0$. Furthermore the denominator is zero $b_{10} = 4$. The

expression for b_{11} is then obtained by setting also the numerator equal to zero in order to remove the singularity at that support point.

This is related to the case analysed in the previous section for the asymptotic expansion $x_2 = q(x_1, \varepsilon)$ at $q(\bar{x}_1, \varepsilon)$ for coefficient q_1 given in (34) where this expression was also unbounded. Now, because we have more freedom we can take b_{11} so that the expression stays bounded at this point. The expression $b_{11} = 100/27$ is obtained by substitution of the equilibrium value for $x_1 = \bar{x}_1 = 3/8$ given by (14) into (45).

Further recursion gives higher order approximations, again first r_n with b_{n-1} then r_{n+1} with b_n and so on. We calculated the following fourth order approximation

$$b_1(\varepsilon) = b_{10} + \varepsilon b_{11} + \varepsilon^2 b_{12} + \dots ,$$

$$b_1(\varepsilon) = 4 + \varepsilon \frac{100}{27} + \varepsilon^2 \frac{58700}{2187} + \varepsilon^3 \frac{80536900}{177147} + \varepsilon^4 \frac{171270040300}{14348907} . \quad (47)$$

In Fig. 11 besides the shape of the limit cycles for two values $b_1 = 4.04019$ (small limit cycle) and $b_1 = 4.04061$ (big limit cycle) also the result of the extended asymptotic expansion $r(x_1, \varepsilon)$, where $\varepsilon = 0.01$, (41) with $b_1 = 4.0403$ is shown. The approximation for $\mathcal{M}_\varepsilon^1$ follows the limit cycle closely up-to a separation point where the small limit cycle bends toward the nullcline which is crossed where the rate of x_1 changes sign and the rate becomes fast. This occurs for the smallest $b_1 = 4.04019$ -value. For the big limit cycle at $b_1 = 4.04061$, from the separation point the trajectory along the cycle continuous to move toward the vertical axis. The asymptotic expansion for $\mathcal{M}_\varepsilon^1$ with $b_1 \approx 4.0403$ continuous after the separation point between the two limit cycles before the approximation becomes unbounded.

These results show how the unique stable limit cycle changes its shape very abruptly when $b_1 \approx 4.0403$ is varied keeping ε fixed, here in our example 0.01: the canard explosion. That the iteration process converges to this bifurcation parameter value where the approximation of the asymptotic expansion $r(x_1, \varepsilon)$ works for the limit cycle with the small amplitude that intersect with the parabolic f-nullcline vertically at the minimum predator size during the limit cycle. This makes in plausible that the iteration procedure yields indeed the canard point.

However, the extended asymptotic expansion $r(x_1, \varepsilon)$ (41) is divergent as shown in Fig. 13 where the coefficients b_{1i} as function of i is depicted.

It was shown in [39, 38] and reference therein, that the summation up to the smallest term gives an optimal (and very accurate) approximation in the case of the van der Pol system. In Fig. 14, again with allochthonous prey input where $\delta = 0.0001$, the parameter value where the explosion occurs is plotted. This b_1 parameter value is taken from Fig. 10. Fortunately, the result presented are in agreement.

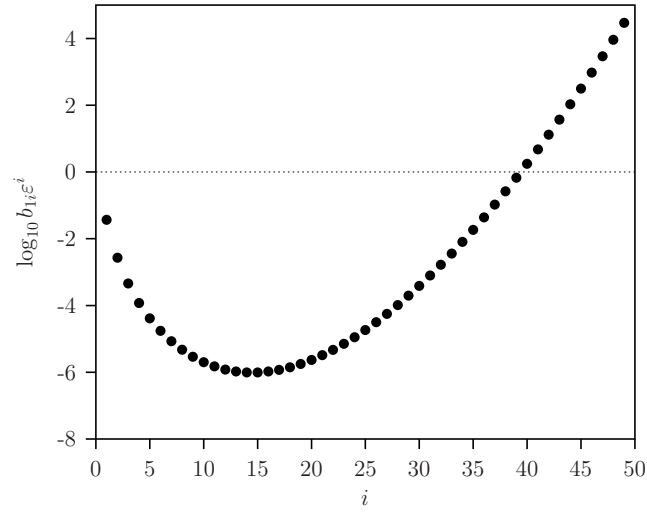


Figure 13: Coefficients b_{1i} as function of i given by (47) with $\varepsilon = 0.01$.

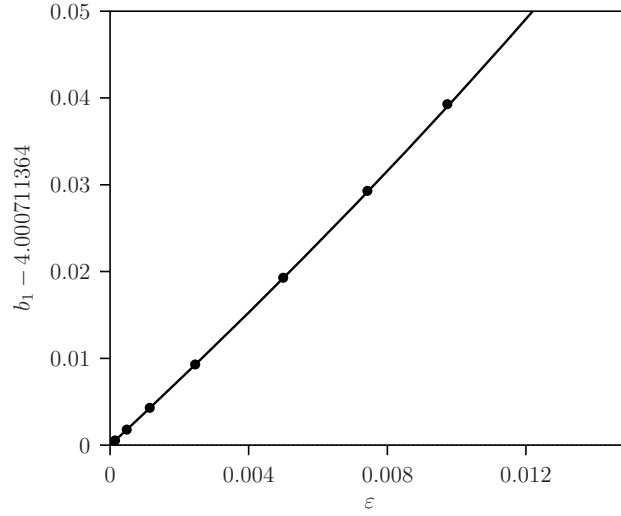


Figure 14: Distance from parameter value b_1 where canard explosion occurs from $b_1 = 4.000711364$ where the Hopf bifurcation occurs with allochthonous prey input $\delta = 0.0001$ as function of ε . Solid line is graph of the truncated expression (43) and the dots taken from Fig. 10.

4 The MB bitrophic food chain model

This section presents the Monod chemostat model [34, 45, 24, 26]. In this model the nutrients consumed by the prey are modelled explicitly instead of using a logistic growth model for the growth of the prey in absence of the predator. Let $x_0(t)$ denote the density of the nutrient, and $x_i(t) \in \mathbb{R}_+$, $t \geq 0$, $i = 1, 2$ the biomass densities of prey and predator, respectively. The scaled version of the Monod model reads

$$\frac{dx_0}{dt} = (x_r - x_0)D_1 - a_0x_0x_1, \quad (48a)$$

$$\frac{dx_1}{dt} = a_0x_0x_1 - D_1x_1 - \frac{a_1x_1x_2}{1 + b_1x_1}, \quad (48b)$$

$$\frac{dx_2}{dt} = e_1 \frac{a_1x_1x_2}{1 + b_1x_1} - D_1x_2. \quad (48c)$$

where x_r is the concentration of nutrient in the reservoir and D_1 the dilution rate, the rate at which the nutrient enters and all trophic levels are exported from the chemostat reactor. The second term of (48a) and the first term of (48b) model the Lotka-Volterra functional response at the prey-nutrient level. The first term of (48c) and the last term on the right-hand sides of (48b) represent the Holling type II functional response. The efficiency e_1 is the ratio of these two terms. For simplicity we assume $e_1 = 1$ and $a_0 = 1$.

It can be shown that all solutions system (48) starting in the non-negative cone eventually lie in the set

$$\Omega = \{x = (x_0, x_1, x_2) \in \mathbb{R}_+^3 : x_0 + x_1 + x_2 \leq x_r\}. \quad (49)$$

So, the asymptotic behavior of system (48) is bounded by x_r . It is possible to decouple this system by the introduction of the function

$$H(t) = x_0(t) + x_1(t) + x_2(t) - x_r, \quad t \geq 0. \quad (50)$$

This gives

$$\frac{dH}{dt} = -D_1H, \quad (51a)$$

$$\frac{dx_1}{dt} = (H + x_r - x_1 - x_2)x_1 - D_1x_1 + D_1\left(\frac{a_1x_1x_2}{1 + b_1x_1}\right), \quad (51b)$$

$$\frac{dx_2}{dt} = D_1x_2\left(\frac{a_1x_1}{1 + b_1x_1} - 1\right). \quad (51c)$$

When furthermore $H = 0$ for the asymptotic dynamics we can study the two dimensional predator-prey system

$$\frac{dx_1}{dt} = x_1 \left(x_r - x_1 - x_2 - D_1 - D_1 \frac{a_1 x_2}{1 + b_1 x_1} \right), \quad (52)$$

$$\frac{dx_2}{dt} = D_1 x_2 \left(\frac{a_1 x_1}{1 + b_1 x_1} - 1 \right). \quad (53)$$

In order to be able to make a clear comparison with the RM-model formulations possible we use $x_r = 1 + D_1$. This gives with $D_1 = \varepsilon$

$$\frac{dx_1}{dt} = x_1 \left(1 - x_1 - x_2 - \varepsilon \frac{a_1 x_2}{1 + b_1 x_1} \right), \quad (54a)$$

$$\frac{dx_2}{dt} = \varepsilon x_2 \left(\frac{a_1 x_1}{1 + b_1 x_1} - 1 \right). \quad (54b)$$

We call this the MB-model. One main difference with the RM-model is that the last term of (54a) is proportional to ε and consequently the efficiency, is constant. Another difference with the RM-model is that the logistic prey growth equation $x_1(1 - x_1)$ is replaced by the expression $x_1(1 - x_1 - x_2)$ with one extra term namely that of the predator biomass, x_2 . In absence of the predator, $x_2 = 0$, both expressions for the prey growth are the same. For the three trophic system including the nutrients, which is used with the derivation of the MB-model, the biomass allocated in the predator gives a feed-back mechanism so that there is less nutrient available for the prey. In the food chain the predator has two adverse effects on the growth of prey population. Firstly the prey is consumed by the predator and they consume building-block material not only for themselves but also for their predators population that can only exists when the prey exists in the absence of inter-guild predation.

The biological interpretation of the $-D_1 H = -\varepsilon H$ term in (51a) is the difference between the influx rate and the out-flux rate of the total biomass expressed in the biomass of the predator. In [45] (50) is used to show that Monod's model is dissipative and that the system converges asymptotically to the manifold $H = 0$ where the influx rate and out-flux rate of the total biomass are the same. Observe that where $H = 0$ there is with respect to the RM-model a new x_2 term in the expression for the prey growth rate.

4.1 Existence and stability analysis of equilibria and limit cycles

For the analysis of model in the chemostat environment we refer to [45]. The three relevant equilibria are summarized in Table 2. In Table 3 the bifurcation analysis results are given. Important difference of these results with those for the RM-model is that while the expressions for the TC bifurcation are the same those for the Hopf H bifurcation still depends on ε .

Firstly we calculate by continuation of the parameter b_1 the bifurcation diagram shown in Fig. 15. This diagram looks very much the same as Fig. 1 for the RM model. The main difference is that the Hopf bifurcation occurs at a somewhat higher b_1 value.

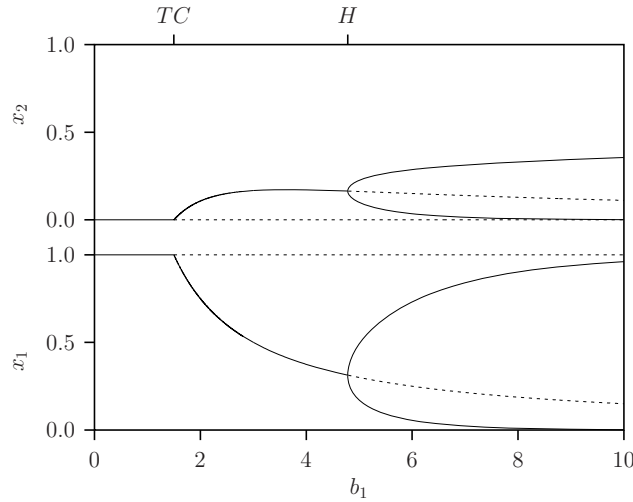


Figure 15: One-parameter bifurcation diagram for b_1 and $a_1 = 5/3 b_1$ of the MB-system (54) with $\varepsilon = 1$.

4.2 Phase-space analysis

Figure 16 displays the simulation results for the MB-model for three values of ε where $b_1 = 3$. There is convergence to a stable equilibrium, similar as we found for the RM-model in Fig. 3a,c.

For $b_1 = 8$ the results are shown in Fig. 17. These results differ much from the RM-model in Fig. 3b,d case where the equilibrium E_2 was unstable. Here this holds true for $\varepsilon = 1$ (Fig. 17a) but for smaller values the equilibrium becomes stable (Fig. 17b,c).

4.3 The degenerate phase point

With $\varepsilon = 0$ substituted in the MB-model (54) there is no input of nutrients (54a) and also no export of the abiotic and biotic elements from the reactor environment. The prey grows logistically to the equilibrium $x_0(0) + x_1(0)$ and the predator population remains constant $x_2(0)$. Hence, the equilibrium E_2 is neutral stable. The degenerate phase curve is just this point which is an equilibrium point x_1 together with the initial predator size $x_2(0)$.

This degenerate phase curve differs completely from that of the RM-model. This is a consequence of the fact that in the MB-model the second term of (54a) is proportional to ε and therefore the ratio of this and the first term of (54b), the efficiency, is constant.

4.4 Bifurcation analysis of MB-model

In order to find-out why this happens we calculated a two-parameter bifurcation diagram shown in Fig. 18 where besides b_1 (whereby $a_1 = 5/3 b_1$), parameter ε is the second variable.

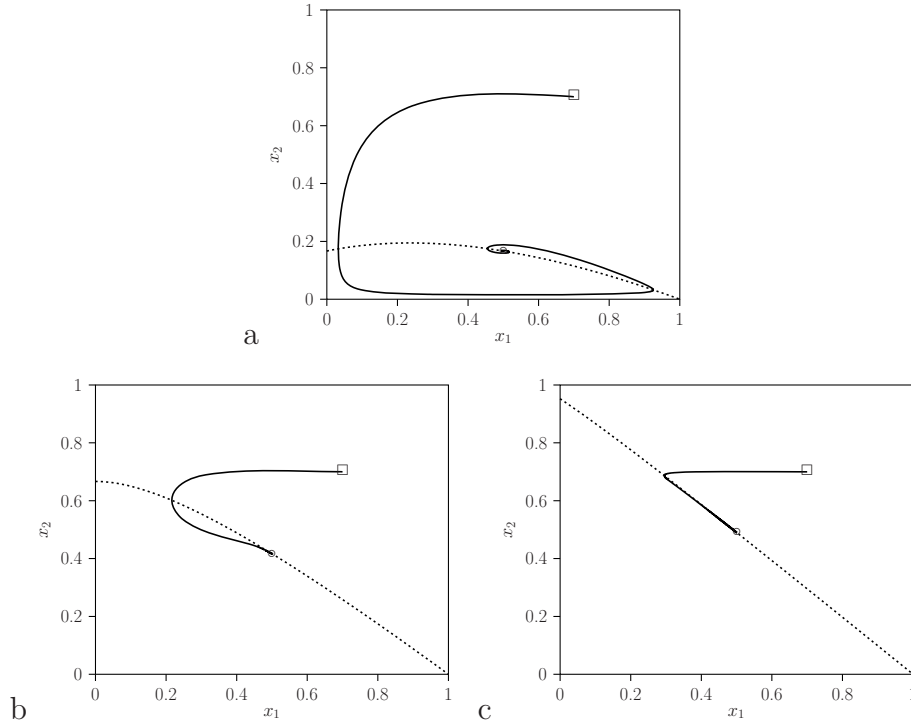


Figure 16: Phase-space analysis for system (54) describing the MB-model with $a_1 = 5/3b_1$, $b_1 = 3$, for three different values of ε : $\varepsilon = 1$, $\varepsilon = 0.1$ and $\varepsilon = 0.01$.

In this diagram the transcritical bifurcation TC , and the Hopf bifurcation H , curves are drawn (see Table 3 for the expressions that describe the curves).

The transcritical bifurcation TC , is the same for all models. This is obviously due to the fact that the model for the dynamics of the predator is the same for all models and furthermore that for the prey-only ($x_2 = 0$) equilibrium E_1 is also the same. For the MB-model the Hopf bifurcation H terminates at the origin where $b_1 \rightarrow \infty$ and $\varepsilon \rightarrow 0$. There is a stable equilibrium E_2 in almost the whole $b_1 > 4$ range up to $\lim b_1 \uparrow \infty$ while in the RM-model there is a stable limit cycle L_2 .

From this we conclude that in the case of the MB-model the parameter ε can not to be used as a single perturbation parameter. We conclude that the complete model has to be analysed using a straight-forward phase-space and bifurcation analysis of the local bifurcations H and TC .

5 Discussion and conclusions

The use of time-scale separation technique has a long tradition in ecology and biochemistry, starting with the quasi-steady-state approximation (QSSA) used to derive the Holling types functional response [17] and Michaelis-Menten kinetics.

In this paper we compared two fast-slow versions of predator-prey models: the RM-

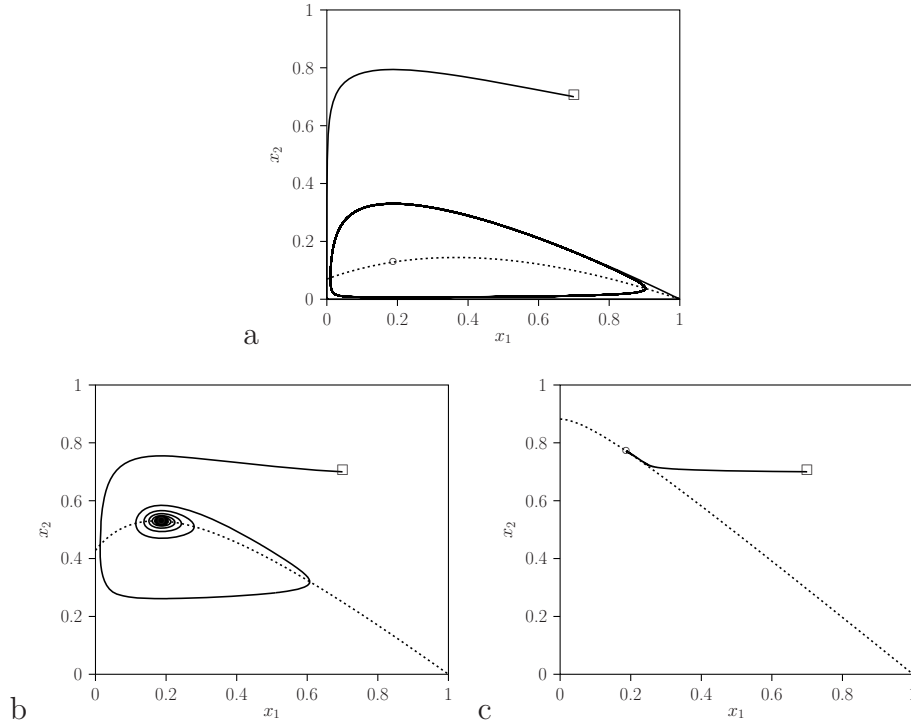


Figure 17: Phase-space analysis for system (54) describing the MB-model with $a_1 = 5/3 b_1$, and $b_1 = 8$, that is at the Hopf bifurcation point for three different values of ε : $\varepsilon = 1$, $\varepsilon = 0.1$ and $\varepsilon = 0.01$.

model and MB-model. In the classical RM-model the small perturbation parameter is proportional to the efficiency of the predator-prey trophic interaction and the predator death rate. In a series of papers [35, 42, 41] the dynamics of this bitrophic systems has been studied intensively.

In [11] this subject was also studied focusing on the dynamics close to the critical manifold \mathcal{M}_0^0 (Fig. 5) (part of the vertical axis where the prey is absent) and related to a delayed (transcritical) bifurcation phenomenon. Recently in [16] the analysis technique based on the geometric singular perturbation theory was applied. This theory can also be used where the interior equilibrium is unstable and relaxation dynamics occurs.

We used the invariant manifold criterion together with an extended asymptotic expansion with respect to both, the perturbation parameter and the free bifurcation parameter. This gives an iteration process that approximates the $\mathcal{M}_\varepsilon^1$ slow manifold close to the parabolic critical manifold \mathcal{M}_0^1 in the neighbourhood of its top. In the parameter range just above the Hopf bifurcation where stable limit cycles exist, this process converges to the point where the canard explosion occurs. In [2] a similar method has been used: here the advantage is that all calculations are done in Maple, [32] with rational numbers.

Direct application, however, showed that the delayed transcritical bifurcation dynamics close to the critical manifold \mathcal{M}_0^0 leads to an disturbing effect because the prey population

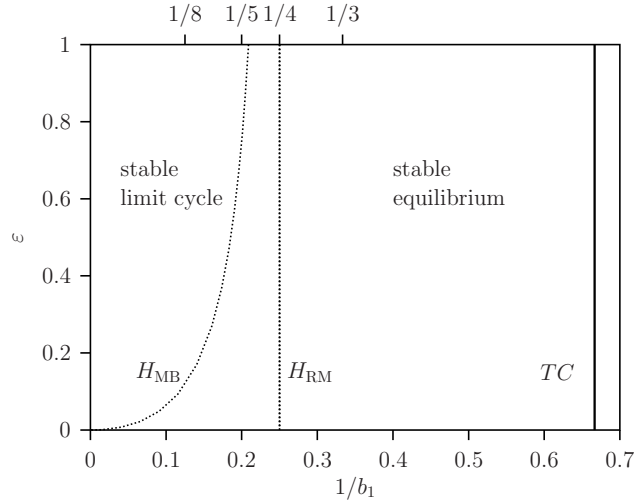


Figure 18: Two-parameter bifurcation diagram with ε and $1/b_1$ as free parameters. The expressions are given in Table 3. The transcritical bifurcation curve TC is for both models RM-model and MB-model the same. For $\varepsilon = 1$ the point of the Hopf bifurcations differ slightly but for $\lim \varepsilon \downarrow 1$ they differ essentially. In the MB-model there is a stable equilibrium E_2 in almost the whole $b_1 > 4$ range up to $\lim b_1 \uparrow \infty$ while there is a stable limit cycle L_2 in the RM-model.

becomes very low. Therefore we introduced a small allochthonous input of prey in which case the non-generic transcritical bifurcation disappears. In [46] the uniqueness of the limit cycles in the RM-model with prey immigration is shown that supports the applicability of this additionally introduced mechanism.

The canard phenomenon found can be described as follows. Also for small perturbation parameter values the trajectories follow the stable limit cycles like in the case where no time scale differences occur $\varepsilon = 1$. However, just above the Hopf bifurcation point depending also on the perturbation parameter the stable limit cycle with small amplitude consists of two concatenated slow and fast episodes. In the phase space, the top part is just above the parabolic stable and unstable critical manifold and the bottom just below the horizontal line connecting the two points where the limit cycle intersects with the f-nullcline vertically. At the canard point of the bifurcation parameter, the dynamics tends abruptly toward the relaxation dynamics. This transition point resembles what happens due to the delayed bifurcation effect where the trajectory leaves the vertical axis below the transcritical bifurcation TC in Fig. 5. For higher bifurcation parameters values the limit cycle with large amplitude changes smoothly and approaches the degenerated phase curves consisting of a concatenation of two slow and two fast episodes (Fig. 5).

Despite the approximate series expansion diverges, we found accurate approximations for small ε of the part the limit cycles originating from the Hopf bifurcation point. Furthermore, the numerical approximate asymptotic iterative scheme, gives very good approximations of the bifurcation parameter b_1 and perturbation parameter ε values where a canard explosion occurs (see Fig. 11).

An other mathematical method to analyse a canard explosion is the blow-up technique [8, 9, 29, 30]. This technique can be used to study the unfolding of the degenerated Hopf bifurcation where $\lim \varepsilon \rightarrow 0$. This will be the subject of a forthcoming paper.

In [35, 42, 41, 20, 16, 11] the RM-model predator-prey slow-fast model showed complex relaxation oscillation dynamics, however, no canard explosion was observed.

In [26, 1, 23] food chain systems were already studied where the small parameter, measuring the timescale disparity between the rate of changes in the prey (fast) and predator (slow), in the MB-model was introduced. Then the fast subsystem converges to a critical manifold of stable equilibria which yields an algebraic relationship between the state variable leading to a reduced (aggregated) lower dimensional (DAE) system. Predator prey systems with fast oscillating migrations were studied in [36] and with slow migrations in [33] wherein reduction methods were proposed. In those papers, relaxation oscillations were not discussed.

In the MB-model, conservation of mass is obeyed and therefore it is more realistic than the RM-model where nutrients are not modelled explicitly. An open chemostat environment is assumed with inflowing nutrients and the outflow of all abiotic and biotic components. Under specific situations the logistic growth rate of the prey is replaced by a prey growth model whereby nutrients are not only used for its own growth but also for its predator. This is a bottom-up effect in addition to the top-down effect of the prey consumption by the predator. The consumption occurs with a constant efficiency like in the alternative fast-slow version of the RM-model introduced in [16, Example 2.2]. The introduction of this constant efficiency in the fast-slow RM-model, however, leads to unrealistic equilibrium population sizes when ε becomes small. In the MB-model (54) these sizes remain realistic. A constant efficiency, instead of the less realistic variable efficiency, was earlier used in [26] in the fast-slow version of the RM-model and described by (2) [16, Example 2.1].

The dynamics of the MB-model was analysed using a classical phase-space and bifurcation analysis approach where only equilibria and limit cycles occur in the whole parameter space. Calculations showed that in this more realistically and mechanistically underpinned model the complex fast-slow canard explosion does not occur.

References

- [1] P. Auger, R. Bravo de la Parra, J-C. Poggiale, E. Sanchez, and L. Sanz. Aggregation methods in dynamical systems and applications in population and community dynamics. *Phys Life Rev*, 5(2):79–105, 2008.
- [2] M. Brons. An iterative method for the canard explosion in general planar systems. *Discrete and continuous dynamical systems*, 250:77–83, 2013.
- [3] M. Canalis-Durand. Formal expansion of van der pol equation canard solutions are gevrey. In E. Benoît, editor, *Dynamic Bifurcation*, pages 28–39. Springer, 1990.
- [4] K.-S. Cheng. Uniqueness of a limit cycle for predator-prey system. *SIAM Journal on Mathematical Analysis*, 12:541–548, 1981.

- [5] B. Deng. Food chain chaos with canard explosion. *Chaos*, 14(4):1083–1092, 2004.
- [6] M. Diener. The canard unchained or how fast/slow dynamical problems bifurcate. *The Mathematical Intelligencer*, 6:38–49, 1984.
- [7] E. J. Doedel and B. Oldeman. Auto 07p: Continuation and bifurcation software for ordinary differential equations. Technical report, Concordia University, Montreal, Canada, 2009.
- [8] F. Dumortier and R. Roussarie. *Canard cycles and center manifolds*, volume 121 of *Memoires of the American Mathematical Society*. American Mathematical Society, AMS, Providence, RI, USA, 1996.
- [9] F. Dumortier and R. Roussarie. Geometric singular perturbation theory beyond normal hyperbolicity. In C. K. R. T. Jones and A. I. Khibnik, editors, *Multiple Time Scale Dynamical Systems*, volume 122 of *IMA*, pages 29–64. Springer-Verlag, Berlin, 2000.
- [10] W. Eckhaus. Relaxation oscillations including a standard chase on french ducks. In *Asymptotic analysis II*, volume 985 of *Lecture Notes in Mathematics*, pages 449–494, Berlin, 1983. Springer-Verlag.
- [11] C. Lobry F. Campillo. Effect of population size in a predator-prey model. *Ecol Model*, 246:1–10, 2012.
- [12] N. Fenichel. Geometric singular perturbation theory. *JDE*, 31:53–98, 1979.
- [13] J-M. Ginoux and J. Llibre. Flow curvature method applied to canard explosion. *J. Phys. A Math. Theor.*, 44(46):465203, 2016.
- [14] J. Guckenheimer. *Normal Forms, Bifurcations and Finiteness Problems in Differential Equations*, volume 137 of *NATO Sci. Ser. II Math. Phys. Chem.*, chapter Bifurcations of relaxation oscillations, pages 295–316. Kluwer, Dordrecht, The Netherlands, 2004.
- [15] J. Guckenheimer and P. Holmes. *Nonlinear Oscillations, Dynamical Systems and Bifurcations of Vector Fields*, volume 42 of *Applied Mathematical Sciences*. Springer-Verlag, New York, 2 edition, 1985.
- [16] G. Hek. Geometric singular perturbation theory in biological practice. *J Math Biol*, 60:347–386, 2010.
- [17] C. S. Holling. Some characteristics of simple types of predation and parasitism. *Canadian Entomologist*, 91:385–398, 1959.
- [18] F. C. Hoppensteadt. *Analysis and Simulation of Chaotic Systems*. Applied Mathematical Sciences. Springer-Verlag, Berlin, 1993.
- [19] S.-B. Hsu. On global stability of a predator-prey system. *Math Biosci*, 174(1-2):1–10, 1978.
- [20] S.-B. Hsu and J. Shi. Relaxation oscillation profile of limit cycle in predator-prey system. *Discrete and continuous dynamical systems series B*, 11(4):893–911, 2009.

- [21] C. K. R. T. Jones. Geometric singular perturbation theory. *Dynamical Systems*, 1609:44–118, 1995.
- [22] J. Kevorkian and J.D. Cole. *Multiple Scale and Singular Perturbation Methods*, volume 114 of *Applied Mathematical Sciences*. Springer-Verlag, Berlin, 1995.
- [23] B. W. Kooi. Modelling the dynamics of traits involved in fighting-predators-prey system. *J Math Biol*, 71:1575–1605, 2016.
- [24] B. W. Kooi, M. P. Boer, and S. A. L. M. Kooijman. Consequences of population models on the dynamics of food chains. *Math Biosci*, 153(2):99–124, 1998.
- [25] B. W. Kooi, J. C. Poggiale, and P. Auger. Aggregation methods in food chains. *Math. Comp. Mod.*, 27(4):109–120, 1998.
- [26] B. W. Kooi, J. C. Poggiale, P. Auger, and S. A. L. M. Kooijman. Aggregation methods in food chains with nutrient recycling. *Ecol Model*, 157(1):69–86, 2002.
- [27] M. Kot. *Elements of Mathematical Ecology*. Cambridge University Press, Cambridge, 2001.
- [28] M. Krupa and P. Szmolyan. Geometric analysis of the singularly perturbed fold. In J. K. R. T. Christopher and A Khibnik, editors, *Multiple-Time-Scale Dynamical Systems*, volume 122 of *The IMA Volumes in Mathematics and its Applications*, pages 89–116. Springer, 2001.
- [29] M. Krupa and P. Szmolyan. Relaxation oscillation and canard explosion. *Journal of Differential Equations*, 174:312–368, 2001.
- [30] C. Kuehn. *Multiple Time Scale Dynamics*, volume 191 of *Applied Mathematical Sciences*. Springer-Verlag, New York, 2015.
- [31] Yu. A. Kuznetsov. *Elements of Applied Bifurcation Theory*, volume 112 of *Applied Mathematical Sciences*. Springer-Verlag, New York, 3 edition, 2004.
- [32] Maple. *Maple software*. Maplesoft, Waterloo, Ontario, Canada, 2008.
- [33] M. Marva, J-C. Poggiale, and R. Bravo de la Parra. Reduction of slow-fast periodic systems with applications to population dynamics models. *Mathematical Models and Methods in Applied Sciences*, 22(10), 2012.
- [34] J. Monod. *Recherches sur la croissance des cultures bacteriennes*. Hermann, Paris, 1942.
- [35] S. Muratori and S. Rinaldi. Low- and high-frequency oscillations in three-dimensional food chain systems. *SIAM J Appl Math*, 52:1688–1706, 1992.
- [36] J. C. Poggiale and P. Auger. Fast oscillating migrations in a predator-prey model. *Mathematical Models & Methods in Applied Sciences (M3AS)*, 6(2):217–226, 1996.
- [37] J. C. Poggiale, P. Auger, F. Cordoleani, and T. Nguyen-Huu. Study of a virus-bacteria interaction model in a chemostat: application of geometrical singular perturbation theory. *Philos T Roy Soc B*, 367:4685–3428, 2009.

- [38] J. P. Ramis. Les développements asymptotiques après poincaré : continuité et... divergences. *La gazette des mathématiciens*, 134:17–36, 2012.
- [39] J. P. Ramis. Poincaré et les développements asymptotiques. *La gazette des mathématiciens*, 133:33–72, 2012.
- [40] C. H. Ratsak, S. A. L. M. Kooijman, and B. W. Kooi. Modelling the growth of an oligochaete on activated sludge. *Wat. Res.*, 27(5):739–747, 1993.
- [41] S. Rinaldi and A. Gragnani. Destabilizing factors in slow-fast systems. *Ecol Model*, 180:445–460, 2004.
- [42] S. Rinaldi and S. Muratori. Slow fast limit-cycles in predator prey models. *Ecol Model*, 61(3-4):287–308, 1992.
- [43] M. L. Rosenzweig. Paradox of enrichment: destabilization of exploitation ecosystems in ecological time. *Science*, 171:385–387, 1971.
- [44] M. L. Rosenzweig and R. H. MacArthur. Graphical representation and stability conditions of predator-prey interactions. *Am Nat*, 97:209–223, 1963.
- [45] H. L. Smith and P. Waltman. *The Theory of the Chemostat*. Cambridge University Press, Cambridge, 1994.
- [46] J. Sugie and Y. Saito. Uniqueness of limit cycles in a Rosenzweig-MacArthur model with prey immigration. *SIAM J Appl Math*, 72(1):299–316, 2012.
- [47] B. Van der Pol. On relaxation oscillations. *Philosophical Magazine*, 7:978–992, 1926.
- [48] G. A. K. van Voorn and B. W. Kooi. Combining bifurcation and sensitivity analysis for ecological models. *Eur. Phys. J. Special Topics*, 226:2101–2118, 2017.

A Derivation of the dimensionless RM-model

From [48] we recall (after some adjustments of the notation), that the classical RM-model is given as

$$\frac{dX_1}{dT} = RX_1(1 - X_1/K) - AF(X_1)X_2, \quad (55a)$$

$$\frac{dX_2}{dT} = (CAF(X_1) - M)X_2, \quad (55b)$$

where $F(X_1) = X_1(1 + AkX_1)^{-1}$ is the well-known Holling type II functional response, with X_j the state variables, k handling time, A the attack rate, C a conversion efficiency, M the predator removal rate (mortality, maintenance, and harvesting), and T is time. A list of symbols is given in Table 4.

This model can be rescaled by using $t = TR$, $x_1 = x_1/K$, and $x_2 = X_2/K$. Note that in the last transformation for the predator biomass differs from [48] to let the efficiency C not disappear in the dimensionless formulation and to be able to deal with the time-scale difference in the fast-slow system the subject here.

Table 4: List of symbols used for RM-model with dimension with their meaning. the biomass of both populations have the same dimension.

Symbol	Meaning
T	Dimensional time
t	Dimensionless time
X_j	Dimensional state variable, indicated by j
x_j	Dimensionless state variable, indicated by j
R	Intra-specific growth rate
A	Attack rate
$F(X_1)$	Functional response, non-dimensional
C	Efficiency, conversion yield, non-dimensional
M	Mortality rate per unit of time
k	Handling time

The non-dimensional model then reads

$$\frac{dx_1}{dt} = x_1 (1 - x_1) - \frac{a_1 x_1}{1 + b_1 x_1} x_2 , \quad (56a)$$

$$\frac{dx_2}{dt} = x_2 \left(\frac{c_1 a_1 x_1}{1 + b_1 x_1} - d_1 \right) , \quad (56b)$$

where $a_1 = AK/R$, $b_1 = kAK$, $c_1 = C$ and $d_1 = M/R$.

B The slow dynamics on the parabola part of the f -nullcline

We give the results for the slow dynamics in the degenerated case $\varepsilon = 0$ where the dynamics is on a part of the f -nullclines critical manifolds.

The slow dynamics on the vertical axis is described again by the system (12). We will now focus on the slow dynamics on the parabola shown in Fig. 19 where the dynamics of the reduced system (21) is solved numerically, yielding the prey population size $x_1(\tau)$ while (20) is used to get the associated predator population size $x_2(\tau)$. Figure 19a gives the results for the stable equilibrium E_2 , $b_1 = 3$ where $a_1 = 5/3$ $b_1 = 5$ case with initial condition $x_2(0) = 0.225$. This value is below point T , where $x_2 = 0.25$. In this case there are two valid initial points given by (19). Starting at the largest x_1 prey value on the right-hand parabolic branch there is convergence toward the equilibrium E_2 . But at the lowest prey value on the left-hand branch there is convergence to the trivial zero-solution where $x_1 = 0$ and $x_2 = 0$.

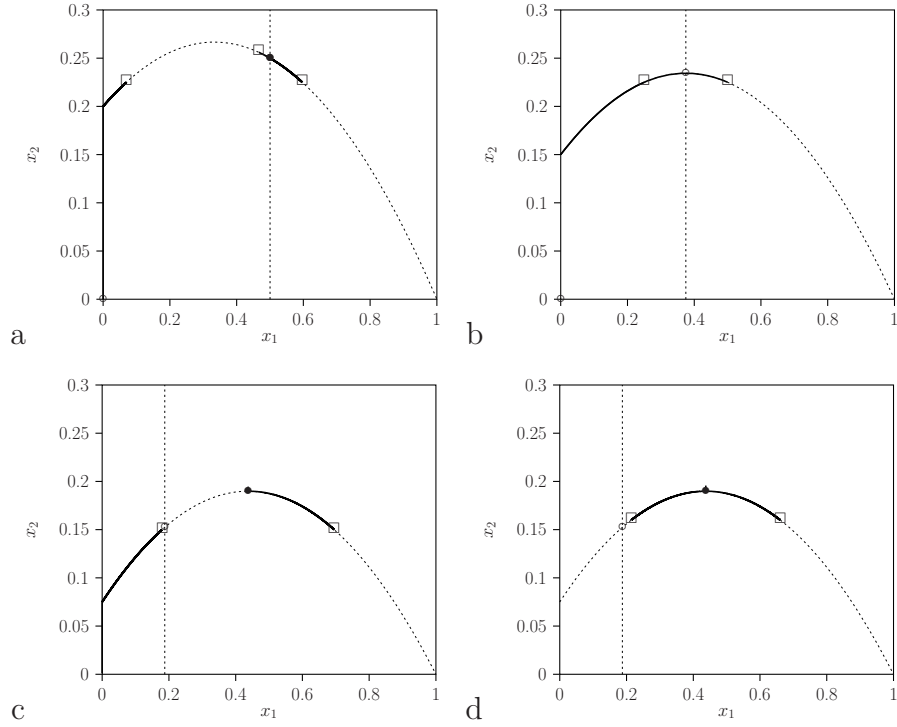


Figure 19: Phase-space analysis for slow system (19) of the RM-model. (a): At the top-panel left $b_1 = 3$ and $a_1 = 5/3 b_1$, with initial values $x_2 = 0.225$ and $x_2 = 0.256$. The equilibrium E_2 is stable and the right-branch of the parabola is the basin of attraction. On the other hand the left-branch of the parabola is in the attraction basin of the zero solution. (b): At the top-panel right $b_1 = 4$ and $a_1 = 5/3 b_1$, with initial values $x_2 = 0.225$. The equilibrium E_2 is unstable. (c) and (d): The lower panel with $b_1 = 8$ and $a_1 = 5/3 b_1$ the two initial values $x_2 = 0.15$ and $x_2 = 0.16$. The associated initial value of the $x_1(0)$ is for $x_2 = 0.15$ below the unstable equilibrium E_2 value. For $x_2 = 0.16$ the associated initial value of the $x_1(0)$ is above the unstable equilibrium E_2 value.

Hence, the right-hand branch of the parabola is in the basin of attraction of the stable equilibrium of the reduced system equal to that of the original system E_2 . On the other hand for the left-hand branch it is in the basin of attraction of the zero solution.

Figure 19c,d were calculated with parameter values $b_1 = 8$ and $a_1 = 5/3 b_1 = 40/3$ where the equilibrium E_2 of the original system is unstable. In Fig. 19c starting at the lowest prey value and $x_2(0) = 0.15$, the results are similar to that in the above discussed case. However, starting with the largest prey value on the critical manifold there is convergence to the limit point T for the reduced system, and not to the unstable equilibrium E_2 of the full model. Note that the vector field is not defined at the top T . In Fig. 19d the initial value is $x_2(0) = 0.16$ where both simulations terminate at a limit point T of the reduced system. Hence, the unstable equilibrium E_2 of the full system is a separatrix between the two equilibrium points of the reduced system, being limit point T in (13) and the zero point $E_0(x_1, x_2) = (0, 0)$.

For the special case $b_1 = 4$ at the Hopf bifurcation the results are shown in Fig. 19b. The equilibrium E_2 of the full system (2) at point T in (14) is now for the reduced system restricted to the critical manifold not an equilibrium of the reduced system and there is no convergence to that point. Starting for $x_2(0) = 0.225$ there is always convergence to the trivial zero solution E_0 which is here a global stable equilibrium of the reduced system.

In order to study the dynamics at the critical manifold (the parabola) further we plot dx_1/dt versus $x_1(t)$ in Fig 20 in addition to $x_2(t)$ versus $x_1(t)$ in the phase space. For the

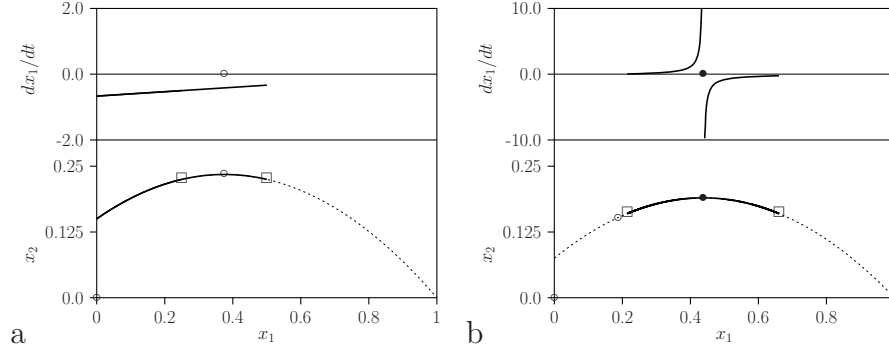


Figure 20: Phase-space analysis for slow system (19) of the RM-model. In the top-subpanels the rate dx_1/dt versus $x_1(t)$ while in the bottom-subpanel the dynamics $x_2(t)$ versus $x_1(t)$ on the critical manifold (see also Fig 19). (a): The left-panel $b_1 = 4$ and $a_1 = 5/3 b_1$, with initial value $x_2 = 0.225$ where the equilibrium E_2 is stable. (b): The right-panel with $b_1 = 8$ and $a_1 = 5/3 b_1$ the initial value is $x_2 = 0.16$ whereby the associated initial value of the $x_1(0)$ is above the unstable equilibrium value.

Hopf bifurcation value $b_1 = 4$ the rate dx_1/dt given in (21) is always negative and hence there is convergence always to the global stable zero solution. Note that the numerator in (21) is zero and this does not hold when $b_1 \neq 4$. However, for $b_1 = 8$ where the equilibrium is unstable the situation differs. Now when starting on the left side of point T the rate dx_1/dt is positive and there is convergence toward the limit point T given in (13). Similarly starting on the right-side the rate dx_1/dt is negative and there is also convergence toward T . Now, the plot shows a vertical asymptote. Thus the rate is discontinuous at point T and this is due to the fact that dq/dx_1 (20) is zero at T . Calculations showed that the equilibrium point of the reduced system is reached in finite time. This is proved in the Appendix B.

In summary, the computational results show that point T is in the case of the reduced system not a simple tangent bifurcation. When the parameter equals the Hopf bifurcation value it is not even an equilibrium. Otherwise it is a limit point reached in finite time.

To support this the dynamics of the RM-model (2) on the parabola, the \mathcal{M}_0^1 part of the f -nullcline (22b) is studied. From equations (20) and (21), one has

$$\frac{dx_1}{d\tau} = \frac{(1 - x_1)((a_1 - b_1)x_1 - 1)}{b_1 - 2b_1x_1 - 1}. \quad (57)$$

804 Since we have :

$$\frac{-2b_1x_1 + b_1 - 1}{(1 - x_1)((a_1 - b_1)x_1 - 1)} = \frac{b_1 + 1}{b_1 + 1 - a_1} \frac{1}{1 - x_1} + \frac{b_1^2 + b_1 - a_1b_1 + a_1}{b_1 + 1 - a_1} \frac{1}{(a_1 - b_1)x_1 - 1}, \quad (58)$$

805 it follows that equation (57) is equivalent to

$$\frac{b_1 + 1}{1 - x_1} + \frac{b_1^2 + b_1 - a_1b_1 + a_1}{(a_1 - b_1)x_1 - 1} dx_1 = (b_1 + 1 - a_1) d\tau, \quad (59)$$

806 thus

$$\int_{x_1(0)}^{x_1(T)} \left(\frac{b_1 + 1}{1 - x_1} + \frac{b_1^2 + b_1 - a_1b_1 + a_1}{(a_1 - b_1)x_1 - 1} \right) dx_1 = \int_0^T (b_1 + 1 - a_1) d\tau, \quad (60)$$

807 where $x_1(T)$ is the coordinate of the top of the parabola: $x_1(T) = \bar{x}_1 = \frac{b_1 - 1}{2b_1}$.

808 If we consider that the equilibrium point ($x_1^* = \frac{1}{a_1 - b_1}$) is at point T , that is at the
809 Hopf bifurcation point when $b_1 = 4$, it follows that: $b_1^2 + b_1 - a_1b_1 + a_1 = 0$.

810 We can then express the time t_T needed for starting from $x_1(0)$ to reach the equilibrium
811 E_2 at point T

$$t_T = \frac{1}{a_1 - b_1 - 1} \left((1 + b_1) \ln \left(\frac{(1 + b_1)/(2b_1)}{1 - x_1(0)} \right) \right). \quad (61)$$

812 But in this case point T is not an equilibrium. If one assumes that the equilibrium is on
813 the right of point T , that is $b_1 < 4$, see Fig. 3a, (60) shows that the equilibrium is not
814 reach in a finite time.

815 Finally, if we assume that the equilibrium x_1^* is on the left of point T that is $b_1 > 4$
816 and if we consider an initial condition between x_1^* and 1, see Fig. 3d, point T attracts the
817 trajectory. It is, however, not an equilibrium in the usual sense because equation (57) does
818 not vanish, it is actually not well defined. Nevertheless this point is reached in a finite
819 time according to (60), and the time needed to reach this point t_T^* is

$$t_T^* = \frac{1}{a_1 - b_1 - 1} \left((1 + b_1) \ln \left(\frac{(1 + b_1)/(2b_1)}{1 - x_1(0)} \right) + \frac{A}{a_1 - b_1} \ln \left(\frac{A/(2b_1)}{(a_1 - b_1)x_1(0) - 1} \right) \right), \quad (62)$$

820 where $A = a_1b_1 - a_1 - b_1^2 - b_1 > 0$ under the above mentioned conditions.